



Quantifying forest structural attributes and aboveground carbon dynamics with terrestrial laser scanning in a temperate deciduous forest

Shilin Chen^{a,*}, Hans Verbeeck^a, Louise Terryn^a, Wout Cherlet^a, Chang Liu^b, Mathias Disney^{c,d}, Yadvinder Malhi^e, Niall Origo^a, Joanne Nightingale^f, Kim Calders^a

^a Q-ForestLab, Department of Environment, Faculty of Bioscience Engineering, Ghent University, Ghent, 9000, Belgium

^b College of Forestry, Beijing Forestry University, Beijing, 100083, China

^c Department of Geography, University College London, London, WC1E 6BT, UK

^d NERC National Centre for Earth Observation, University College London, London, WC1E 6BT, UK

^e Environmental Change Institute, School of Geography and the Environment, University of Oxford, South Parks Road, UK

^f Climate and Earth Observation group, National Physical Laboratory, Teddington, TW11 0LW, UK

ARTICLE INFO

Keywords:

Forest dynamics
Carbon dynamics
Terrestrial laser scanning (TLS)
Point clouds
Quantitative structure model (QSM)

ABSTRACT

Quantifying forest structure and aboveground biomass carbon (AGBC) dynamics over time is crucial for evaluating climate change impact on carbon stocks, and providing key insights into changes in the terrestrial carbon cycle. To date, the use of multi-temporal terrestrial laser scanning (TLS) to detect temporal dynamics of forest structure and AGBC remains largely unexplored. In this study, we demonstrate the use of bi-temporal TLS data to quantify fine-scale dynamics of forest structure and AGBC. A total of 831 live trees were extracted and manually aligned from two leaf-off datasets collected in a 1.4 ha area of temperate woodland (Wytham Woods, UK) in 2016 and 2022. Results indicated that, at the individual tree level, most trees exhibited positive growth in structural attributes between 2016 and 2022, including diameter at breast height (DBH, 60.2 % of trees), tree height (H, 75.8 %), crown projection area (CPA, 64.7 %), crown volume (CV, 60.5 %), and aboveground volume (V, 50.5 %). At the plot level, all structural attributes also increased, including basal area (1.8 m²/ha, 4.8 % growth), H (128.9 m/ha, 1.4 %), CPA (411.9 m²/ha, 3.0 %), DBH (1.5 m/ha, 1.1 %), CV (181.7 m³/ha, 0.3 %), and V (7.9 m³/ha, 1.0 %). The total AGBC of the study area saw a net carbon gain of 0.4 Mg C/ha/year over the six-year period. Notably, trees with DBH greater than 60 cm contributed over 40 % of the total AGBC. Moreover, our results reveal that branch dynamics play a crucial role in AGBC dynamics, underscoring the added value of TLS for tracking AGBC changes over time.

1. Introduction

Quantifying forest dynamics is crucial for studying forest ecosystem processes over time, monitoring terrestrial carbon cycling, mitigating climate change, and developing forest management practices (Chen et al., 2025; McDowell et al., 2020; Schulte et al., 2022). Forest dynamics, including forest growth, loss, and degradation, necessitate timely and accurate monitoring of forest conditions. Conventional forest monitoring has primarily relied on forest inventory measurements, focusing on key tree attributes such as diameter at breast height (DBH), tree height (H), species, and tree location, to form the backbone of ground-based assessments of forest structural changes and biomass carbon dynamics (Coops et al., 2025; Fu et al., 2021). For example, Shen

et al. (2018) utilized two periods (2002 and 2007) of forest inventory data with satellite remote sensing observations, they mapped the spatial distribution of biomass and revealed that biomass in subtropical evergreen broadleaved forest of China showed an increasing trend, whereas tropical forests exhibited a decreasing trend. Similarly, Herraiz et al. (2023) analyzed data from 7000 plots in the 1995 and 2006 Spanish national forest inventories, combined with biomass and productivity models, and predicted that increasing aridity conditions could seriously reduce forest biomass by 18 % and productivity by 16 %. However, emerging evidence suggests that such approaches may overlook several critical components closely linked to forest structure and biomass carbon dynamics, such as small trees (DBH < 10 cm), tree crown, branchfall, trunk breakage, and wood decay, which can substantially

* Corresponding author.

E-mail address: Shilin.chen@ugent.be (S. Chen).

<https://doi.org/10.1016/j.agrformet.2025.110995>

Received 28 August 2025; Received in revised form 12 December 2025; Accepted 14 December 2025

Available online 18 December 2025

0168-1923/© 2025 Elsevier B.V. All rights reserved, including those for text and data mining, AI training, and similar technologies.

influence forest structural complexity and biomass turnover (Needham et al., 2022; Piponiot et al., 2022; Zuleta et al., 2023). Moreover, forest dynamics are changing rapidly due to the increasing disturbances, including wildfire, drought, storm, and biotic attacks, and anthropogenic drivers, such as rising temperatures and carbon dioxide concentration (McDowell et al., 2020). Given the limitations of conventional forest inventory measurement and monitoring methods, such as limited survey structural metrics and insufficient detail on crown changes, accurately and timely quantification of forest dynamics remains a huge challenge (Dalponte et al., 2019). Therefore, it is becoming increasingly important to further develop methods to measure and monitor forest changes (Terryn et al., 2023). Of the current methodologies, remote sensing technology offers a powerful, scalable, and non-destructive method and has been widely used to monitor forest structure and carbon dynamics. Particularly Light Detection and Ranging (LiDAR, or laser scanning) can play a critical role in forest monitoring, due to its ability to capture the three-dimensional (3D) forest structure (Calders et al., 2020; Coops et al., 2025; Li et al., 2024; McCarley et al., 2017; Zhao et al., 2018).

Over recent years, TLS (terrestrial laser scanning) has demonstrated its ability to quantify forest structure and aboveground biomass carbon (AGBC) stock (Calders et al., 2015; Coops et al., 2025; Terryn et al., 2020). Furthermore, numerous studies have demonstrated that TLS point clouds not only allow for the assessment of a wide range of simple tree structural parameters, such as DBH, H, tree location, crown size, and projection area (Bauwens et al., 2016; Calders et al., 2020; Liang et al., 2016; Terryn et al., 2022), but can also be integrated with specialized modelling approaches to derive more complex structural metrics related to the fine-scale tree architecture, thereby fully exploiting the potential of the data. For example, tree point clouds can be used with modelling algorithms to reconstruct 3D quantitative structure models (QSMs) of individual trees, enabling accurate estimates of stem shape, volume, and branch architecture (Calders et al., 2015; Feng et al., 2024). Aboveground biomass (AGB) estimates derived from TLS-QSM approach have consistently shown strong agreement with destructive measurements across different forest conditions, exhibiting less bias and more accurate than those calculated from allometric models (Demol et al., 2022). Furthermore, Calders et al. (2022) quantified AGBC in a typical temperate forest in the UK by reconstructed individual tree QSMs combined with species-specific wood density and carbon density values, revealing that currently used allometric biomass models significantly underestimate the biomass carbon, particularly for large trees (DBH > 53.1 cm), and highlighting critical limitations in traditional forest carbon accounting approaches.

The availability of multi-temporal TLS data provides new opportunities to quantify forest structure and carbon dynamics over time in detail and understand how and why they vary across spatial scales (Calders et al., 2025). Limited studies that used multi-temporal 3D data to quantify forest dynamics have analyzed changes in forest ecosystems at both the individual tree level (Liang et al., 2012; Martin-Ducup et al., 2017; Srinivasan et al., 2014; Wang et al., 2022, 2025) and the plot level (Liu et al., 2024; Yrttimaa et al., 2020). At the individual tree level, Martin-Ducup et al. (2017) used bi-temporal TLS data, collected with a two-year interval, to quantify canopy change by analyzing differences across four metrics extracted from coniferous and broadleaf trees, and revealed that broadleaf trees exhibited a stronger response to gap formation compared to conifers, indicating a more pronounced ability to adapt to changes in canopy structure. Yrttimaa et al. (2022) characterized canopy structure and competition using forest structural parameters extracted from bi-temporal data with a five-year interval, and analyzed stem volume growth. In addition to detecting long-term (multi-year interval) forest dynamics, a few studies have also attempted to track short-term (ranging from a few hours to several months) forest dynamics using hourly or monthly scanning repetition rates. Campos et al. (2021) installed an automated and permanent TLS measurement station in Finland to scan hourly, which provides a unique

dataset to monitor the 3D physical structure of the forest at both short- and long-term scales and brings new insights into forest dynamics. Wang et al. (2022) presented an automated algorithm to quantify structural movements and circadian rhythms of a birch tree with centimeter-level accuracy from hourly scanned data. At plot level, Liu et al. (2024) utilized bi-temporal TLS data in combination with 3D radiative transfer modeling to compare radiative transfer across different time points, explaining the dynamics of the fraction of absorbed photosynthetically active radiation (FAPAR) and canopy light extinction and the impact of canopy gap dynamics on light availability at specific locations. A detailed summary of previous studies that evaluated forest structure or biomass carbon dynamics using multi-temporal TLS data has been summarized in Table 1. Although these studies have explored forest structure dynamics across different scales using multi-temporal data, to date, the quantification of forest carbon dynamics from multi-temporal TLS data combined with QSMs remains largely unexplored.

In this study, we explored the capacity of bi-temporal TLS data to quantify forest structural attributes and AGBC dynamics at both the individual tree and plot levels. Leveraging TLS data collected under leaf-off conditions in 2016 and 2022 from Wytham Woods, a typical temperate forest in the UK, and detailed QSM reconstruction, we extracted key forest structural attributes, including DBH, H, crown projection area (CPA), crown volume (CV), and aboveground tree volume (V), to analyze forest AGBC dynamics. Specifically, the objectives of this study are: i) to extract key tree structural attributes from point clouds (DBH, H, CPA, CV) and QSMs (total V, trunk and branch volume) to measure structure changes and carbon stock dynamics; ii) to investigate the contribution of species and diameter classes to changes in forest structure and carbon stock; iii) to reveal the AGBC dynamics over a six-year period and identify the tree components that contributed the most to these changes. Additionally, structural attributes derived from bi-temporal TLS data were compared with those from traditional forest inventory measurements to assess differences between the two approaches in evaluating forest structural changes. This study explores the strengths of TLS in capturing realistic 3D forest structures and enabling structure change traceability, offering critical insights for the quantification of forest structural attributes and AGBC dynamics using multi-temporal TLS data.

2. Materials and methods

2.1. Study area and data collection

The study site is located in Wytham Woods, a typical UK temperate, mature secondary broadleaved forest, extensively studied for its diverse flora and fauna. Wytham Woods covers an area of 404 ha, including over 20 tree species, but is mainly dominated (approximately 96 %) by five tree species: European ash (*Fraxinus excelsior*), sycamore (*Acer pseudo-platanus*), common hazel (*Corylus avellana*), common hawthorn (*Crataegus monogyna*), and English oak (*Quercus robur*) (Terryn et al., 2020). This site has been owned by Oxford University since 1943 as part of the UK Environmental Change Network (ECN) long-term monitoring site. The mean annual temperature and precipitation are 10 °C and 726 mm, respectively (Butt et al., 2009; Calders et al., 2022). Eighteen hectares of Wytham Woods are designated as part of Forest Global Earth Observatory (Forest GEO) to carry out long-term forest inventories, which is managed and maintained by Oxford University. A 1.4 ha area (100 m × 140 m) within the 18 ha plot is used as our study area, where periodic TLS data acquisition is conducted to monitor forest dynamics of Wytham Woods.

Woodland inventory data was collected in August 2016 and June 2021, respectively (<http://www.yadvindermalhi.org/blog/recensus-of-the-great-plot-at-wytham-woods>). All trees with a DBH greater than 1 cm (tracking the growth dynamics of small trees over time is of great ecological importance) were marked with a unique tree identifier and recorded. Additionally, the DBH, species, and health

Table 1

A summary of previous studies that evaluated forest structure or aboveground biomass carbon dynamics using multi-temporal terrestrial laser scanning (TLS) data.

Previous study	Study area	Dataset (number of trees)	Forest types	TLS instrument	Data acquisition time (times)	Evaluated metrics	Analysis scale	Reported accuracy
Liang et al. (2012)	Evo, Finland	137 (50 harvested)	Boreal managed forest	Leica HDS6000	March and August 2008 (2)	DBH, stem change	Individual	DBH: RMSE=1.29 cm, Stem change detection rate: 90.0 %
Eitel et al. (2013)	Western central Idaho, USA	10	Temperate forest	Self-developed ATLS	12–29, October 2012 (4)	H, canopy height, DBH	Individual	R ² : 0.98–1.00
Srinivasan et al. (2014)	East Texas, USA	78 (58 loblolly pines+ 20 hardwoods)	Planted coniferous forest	Leica ScanStation2	2009–2012 (2)	AGB	Individual	Loblolly pine: Adj-R ² = 0.95, Hardwoods: Adj-R ² = 0.99
Griebel et al. (2015)	Victoria, Australia	3 plots	Dry sclerophyll open forest	VEGNET scanner	1 September 2012 to 31 August 2014 (Daily monitoring)	PAI, PAVD	Plot (0.5 ha)	–
Martin-Ducup et al. (2017)	Quebec, Canada	72 (6 plots)	Temperate, broadleaf, and mixed forests	Faro Focus 3D	2013–2015 (2)	Crown characteristics	Individual	–
Yrttimaa et al. (2020)	Evo, Finland	1280 (37 plots)	Boreal forest	Leica HDS6100, Faro Focus 3D X330	2014–2019 (2)	DBH, BA, H, D-H-ratio, Δ hc, Δ cr	Individual, plot (0.1 ha)	DBH: RMSE=0.99–1.22 cm, BA: RMSE=44.14–55.49 cm ² , H: RMSE=1.91–4.85 m
Bogdanovich et al. (2021)	Extremadura, Western Spain	174 (4 plots)	Mediterranean open woodland	RIEGLVZ-2000	2015–2018 (2)	H, CPA	Individual	H: Median range=3.3 %±2.7 %~5.6 %±3.8 %, CA: Median range=1.0 %±1.6 %~2.0 %±1.9 %
Luoma et al. (2021)	Evo, Finland	736 (37 plots)	Boreal forest	Leica HDS6100, Faro Focus 3D X330	2014–2019 (2)	DBH, H, stem form, stem volume allocation	Individual, plot (0.04 ha)	DBH: RMSE=0.6~1.1 cm, H: RMSE=1.7~5.4 m, stem volume: relative change= 25.4 %
Husin et al. (2022)	Seberang Perak, Malaysia	40	Oil palm plantation	Faro Focus 3D	July–November 2017 (3)	Crown strata number, CPA, frond angle, frond number	Individual	–
Wang et al. (2022)	South Finland, South-eastern England	2 (one birch, one oak)	Temperate deciduous tree	RIEGL VZ-4000, Leica HDS-6100	11–12 September 2013 (22), 2014–2018 (3)	Structural movements	Individual	–
Yrttimaa et al. (2022)	Evo, Finland	218 (16 plots)	Boreal forest	Leica HDS6100, Faro Focus 3D X330	2014–2019 (2)	BA, stem volume, crown characteristics, competition metrics	Individual, plot (0.1 ha)	r > 0.8
Terryn (2024)	Queensland, Australia	57	Tropical rainforest	RIEGL VZ-400, RIEGL VZ-2000i	2018–2023 (2)	DBH, H, CPA, CV	Individual	DBH: median-AG=1.9 cm, H: median-AG=0.29 m, CPA: median-AG=1.0 m ² , CV: median-AG=16.97 m ³
Wang et al. (2025)	Northeastern China	3105 (60 plots)	Coniferous forest	Trimble TX8 RIEGL VZ-400i	2019–2023 (2)	DBH, H, BA, HCB	Individual, plot	Δ DBH: RMSE=0.5~0.82cm Δ BA: RMSE=0.001~0.003m ² Δ H: RMSE=0.57~0.64m Δ HCB: RMSE=0.66~1.31m

ATLS: Autonomously operating Terrestrial Laser Scanner.

DBH: Diameter at Breast Height; H: tree height; AGB: Aboveground Biomass; PAI: Plant Area Index; PAVD: Plant Area Volume Density; BA: Basal Area; CPA: Crown Projection Area; CV: Crown Volume; D-H-ratio: Diameter-Height ratio; Δ hc: height difference of the crown base; Δ cr: crown ratio; HCB: Crown Base Height. RMSE: Root Mean Square Error; Adj-R²: Adjusted R-square; AG: Absolute Growth.**Table 2**

The diameter at breast height (DBH) characteristics based on forest inventory data. The number of individuals per tree species and DBH information (mean, standard deviation (SD), minimum (Min) and maximum(Max)) are given for each tree species.

Species	Number (2016)	DBH (cm, 2016)				Number (2021)	DBH (cm, 2021)			
		Mean	SD	Min	Max		Mean	SD	Min	Max
<i>Fraxinus excelsior</i>	79	24.1	18.1	4.3	98.3	78	25.7	19.4	4.0	102.4
<i>Acer pseudoplatanus</i>	527	23.7	15.5	1.6	141.2	520	24.4	15.7	3.0	141.5
<i>Corylus avellana</i>	43	9.1	2.2	5.5	15.6	43	9.4	2.3	5.6	15.8
<i>Crataegus monogyna</i>	24	10.5	4.8	5.5	25.6	23	10.8	4.7	5.6	25.5
<i>Quercus robur</i>	35	63.2	15.2	39.9	97.0	35	63.8	15.6	39.5	99.3
<i>Acer campestre</i>	2	7.6	0.5	7.1	8.1	2	7.6	0.4	7.2	7.9

status of each tree were recorded. Tree species and health status were primarily determined through visual interpretation by field surveyors. By matching forest inventory data with the TLS data (Calders et al., 2018), 710 trees were identified in 2016, while 701 trees were matched in 2021. A total of 709 trees, including 22 standing dead trees, were consistently recorded in both 2016 and 2021 inventory data. The DBH statistical characteristics are summarized in Table 2.

TLS datasets were collected during leaf-off conditions in the winter of 2016 (December 2015 & January 2016) and 2022 (February & March). Leaf-off point cloud data exhibited less canopy occlusion effects compared to leaf-on data, allowing for more detailed representation of crown structure, particularly in the upper canopy. Moreover, QSMs reconstructed from leaf-off data yield volume estimates that more closely align with destructive measurements than those derived from leaf-on conditions (Calders et al., 2018). Scanning was carried out on a 20 m regular grid, comprising a total of 48 scan locations. At each location, two scans (one vertical scan and one tilted scan at 90 degrees from the vertical) were performed to minimize canopy occlusion effects. The permanent hectare marker helped to scan at approximately the same locations during both acquisitions. Two different RIEGL terrestrial laser scanners (RIEGL Laser Measurement Systems GmbH), a RIEGL VZ-400 and VZ-400i, were used to capture point clouds in 2016 and 2022, respectively. The beam divergence and angular sampling resolution are 0.35 mrad and 0.04°, respectively. Both scanners employed a narrow infrared laser beam with a wavelength of 1550 nm, and were operated at the pulse repetition rate of 300 kHz (Table 3) to ensure data-interoperability.

2.2. Data processing

The raw single-scan data from 2016 to 2022 were imported into RiSCAN PRO software (<http://www.riegl.com/products/software-packages/riscan-pro/>) for co-registration, noise filtering, and other pre-processing steps. The TLS plot-level data were downsampled to a resolution of 0.026 m to eliminate the impact of density difference on structural parameter extraction (Calders et al., 2018). To ensure high-quality individual tree point clouds and avoid errors introduced during tree segmentation, all individual tree point clouds used in this study were subjected to quality assessment of individual-tree point cloud integrity and manual correction of mis-segmented point clouds. The tree segmentation of the 2016 leaf-off point clouds was conducted using the open-source software *Treeseg* (Burt et al., 2019) by Calderys et al. (2018), followed by manual inspection and corrections. The tree segmentation of the leaf-off point cloud from 2022 was manually performed by Liu et al. (2024) using the 2016 individual point clouds as an initial reference. All trees (DBH > 1 cm) within the 1.4 ha study area were segmented, including standing dead trees and stumps. Although the collected point clouds included additional information such as intensity, only the xyz coordinates were considered for our analysis.

Although the TLS point clouds from 2016 to 2022 were acquired

Table 3

The data collection specifications for the terrestrial laser scanning (TLS) instruments used in 2016 and 2022.

Year	TLS 2016	TLS 2022
Laser scanning instrument	RIEGL VZ-400	RIEGL VZ-400i
Collecting date	December 2015 - January 2016	February - March 2022
Wavelength [nm]	1550	1550
Pulse repetition rate [kHz]	300	300
Field of view [°]	100 × 360	100 × 360
Beam divergence [mrad]	0.35	0.35
Maximum measuring range [m]	~600	~800
Measurement accuracy [mm]	5	5
Scanning pattern [m]	20 × 20	20 × 20

using the consistent scanning protocols and location, the scanner placement was not precisely identical. As a result, spatial deviations exist between the two point clouds, and precise alignment at the individual tree level is required to enable accurate analysis of crown structural dynamics. The 2016 point clouds of individual trees served as a spatial reference for implementing manual alignment procedures of their 2022 counterparts, ensuring bi-temporal positional consistency of matched trees, as shown in Fig. A1 (Appendix). Quality control was performed by assessing the overlap congruence between corresponding trunks (particularly the trunk base) and primary branches across bi-temporal datasets from different spatial perspectives. Manual adjustments were made in the xyz directions (with a minimum adjustment unit of 1 cm per move) until achieving good morphological alignment (Fig. A1a). Manual point cloud alignment and visual inspection were performed using the open-source R studio (<https://posit.co/download/rstudio-desktop/>) and CloudCompare (<https://www.danielgm.net/cc/>), respectively. For some trees, significant shape changes due to growth, wind, or other factors made it impossible to achieve accurate alignment of the trunk (defined as the main stem) and main branches. In such cases, manual alignment was primarily based on the registration of the trunk base to ensure accurate positioning (Fig. A1b). In this study, a total of 831 trees were manually aligned across bi-temporal individual tree point clouds. Additionally, compared to 2016, 19 additional trees were recorded as dead in 2022.

2.3. Quantitative structure models (QSMs)

Quantitative Structure Models (QSMs) have been proven to yield accurate estimates of reconstructed tree aboveground volume compared to results obtained from destructive harvesting (Calders et al., 2015; Demol et al., 2021; Fan et al., 2020; Hackenberg et al., 2015; Raunonen et al., 2013; Vandendaele et al., 2024). Among various QSM algorithms, TreeQSM stands as the most widely applied, which constructs 3D tree models by fitting cylinders to identified tree components (e.g., trunks and branches). Cooper (2026) (unpublished results) evaluated the volumetric reconstruction performance of multiple QSM algorithms using datasets from diverse forest types, finding that TreeQSM version 2.0 achieved the strongest agreement with destructive harvest measurements and superior accuracy in the context of tree volume estimation. Therefore, TreeQSM version 2.0 was employed in this study to reconstruct QSMs from manually segmented, leaf-off point clouds collected from Wytham Woods in 2016 and 2022.

The most critical parameter in the TreeQSM algorithm is the cover patch size, which determines the reconstruction model refinement and, consequently, influences the reconstructed volume. Both tree size and species-specific architectural traits can affect the optimal cover patch size selection. To ensure that the model volume for each tree is derived from the reconstruction using the optimal cover patch size, QSMs were generated for each tree using cover patch sizes ranging from 0.02 m to 0.11 m, with an increment of 0.005 m. Following the optimization protocol described by Calderys et al. (2018), the optimal patch size per tree was determined by calculating the mean and standard deviation from the ten QSMs generated for each cover patch value. Once the optimal cover patch size was determined, the final model result was obtained by averaging the ten QSMs reconstructed using this parameter, thereby reducing the uncertainty of the final model results.

2.4. Structural attribute extraction

The dynamic changes in forest structure within the study area over the six-year period from 2016 to 2022 were quantified using key structural attributes. Forest structural attributes, serving as critical biometric indicators for assessing forest structure dynamics, can be derived from both TLS data and reconstructed QSMs. In this study, DBH, H, CPA, CV, and basal area (BA) were extracted from individual point clouds, while trunk volume, branch volume, and V were derived from

QSMs.

The ITSM R package (Terry et al., 2023) was utilized for extraction of DBH, H, CPA, and CV. To eliminate discrepancies in DBH height calculation caused by inconsistencies in trunk base segmentation across different temporal datasets, a normalized height reference system was implemented where the minimum z-coordinate value from a point cloud in 2016 served as the standardized ground reference for 2022 DBH height calculations. Point cloud slices with a thickness of 6 cm, extracted from a height range of 1.27 to 1.33 m above the ground, were used for the fitted-circle DBH and the functional DBH. The DBH fitting results of each tree were manually inspected, and the DBH value from the algorithm that best matched the point cloud slice was selected as the final DBH estimate. Due to factors such as point cloud density, tree size, branch occlusion, and noise, DBH fitting failed for some trees. To address this issue, a manual extraction of the trunk point cloud slice at a height of 1.27 m to 1.33 m was carried out, followed by recalculation using the least-squares circle-fitting algorithm. For trees where DBH could not be successfully extracted, the DBH values derived from the QSMs (i.e., the diameter of the cylindrical segment at DBH location) were adopted instead. For H estimation, a similar approach was employed to mitigate errors introduced by inconsistencies in trunk base segmentation. Specifically, the minimum z-value of the 2016 point clouds were used as a reference for extracting H from the 2022 point clouds.

The crown is defined as the components of a tree above the start of the lowest branch. The CPA is defined as the area enclosed by the convex hull constructed from the individual crown point cloud in the XY plane. The parameter *concavity* is a user-defined value that controls the level of detail in the concave hull (Terry et al. 2023). In this study, *concavity* was set to 1. CV is calculated as the volume of the 3D alpha shape generated from the crown point cloud. Similar to the *concavity* parameter, the *alpha* parameter is a crucial factor controlling the generation of the alpha shape, which was set to 1. Due to the difficulty in extracting crown point clouds for some small trees (DBH < 5 cm), CPA and CV could not be estimated for these trees. As a result, they were excluded from analysis related to CPA and CV.

Changes in BA, defined as the cross-sectional area of all trees at DBH per unit area, over time can provide critical insights into forest structure and biomass carbon dynamics. In this study, the BA was calculated using the DBH values, based on the following formula:

$$BA = \left(\sum_{i=1}^n \frac{\pi (DBH)^2}{4} \right) / (1.4) \quad (1)$$

where *i* is the *i* th tree, *n* is the quantity of alive trees, and 1.4 represents the area of the plot in ha.

2.5. Aboveground biomass carbon estimation

The AGBC of individual trees (DBH>1 cm) and the entire 1.4 ha plot were assessed separately to analyze carbon dynamics. The biomass carbon stock of individual trees was calculated by multiplying the QSM-derived volume with the corresponding wood density and carbon coefficient of that specific species. Wood density and carbon coefficient values for each species were obtained from previous studies (Butt et al., 2009; Fenn et al., 2015) and the global wood density database (Chave

et al., 2009). For unidentified species or species without available wood density and carbon coefficient values, the average values of wood density and carbon coefficients were adopted for biomass carbon estimation. A summary of carbon coefficient, and wood density values for different species is provided in Table 4. The wood density and carbon coefficient of standing dead trees are closely related to tree species, decomposition stage, and environmental conditions, and are generally lower than those of living trees to varying degrees (Herrmann et al., 2015). However, as such information was not available in this study, the biomass carbon stock of standing dead trees was calculated using the wood density and carbon coefficient values of their corresponding living tree species. For unidentified dead trees, the average wood density and carbon coefficient of living trees were used for the estimation. In the Wytham Woods 2016 dataset, the carbon stocks of 850 living trees and 54 standing dead trees were assessed, while in the 2022 dataset, the carbon stocks of 831 living trees and 39 standing dead trees were evaluated. The numbers of living trees of different species in 2016 and 2022 are provided in Table 4. To more clearly and accurately understand the dynamic changes in biomass carbon across different tree components, the AGBC of individual trees was partitioned into trunk and branch components. Although there are slight variations in wood density and carbon coefficients among different tree components, their influence on the biomass carbon estimation for each part was not considered in this study.

The AGBC stock of the plot was obtained by summing the biomass carbon of individual trees, including both live and standing dead trees. The biomass carbon assessment of the plot considered only the above-ground woody components of trees (DBH>1 cm), whereas leaves, belowground tree components, coarse woody debris, shrubs, and herbaceous vegetation were not included.

2.6. Forest structure and biomass carbon dynamics analysis

To quantify forest structure and AGBC dynamics over the six-year period, a comparative analysis was conducted for each forest structural attribute and biomass carbon extracted from the 2016 and 2022 datasets. The analysis was performed at three levels: species-level group, DBH group, and the entire plot level.

To explore the dynamic changes in forest structure and biomass carbon among different tree species, the dataset was categorized into six species-level groups: CRATMO, CORYAV, ACERPS, FRAXEX, QUERRO, and Others. The Others group comprised unidentified species and species with fewer than five individuals. The number of trees included in each species (Matched number) is presented in Table 4. Although the number of individuals varied across species, the analysis of changes in forest structural attributes was primarily based on group mean values to minimize the impact of imbalanced sample sizes. Additionally, the biomass carbon stocks of each species in 2016 and 2022 were calculated to analyze species-specific biomass carbon dynamics over the six-year period.

Trees were classified into seven DBH groups at 10 cm intervals (with all trees having a DBH over 60 cm grouped together, i.e., (0, 10), [10, 20), [20, 30), ..., [60, ~)) to analyze the distributional characteristics, structural changes, and carbon dynamics across different DBH groups. This classification method enables the calculation of three key indicators

Table 4

A summary of living tree populations, carbon density (*c*), and wood density (*ρ*) for different tree species. Number: number of individuals.

Parameter	<i>Crataegus monogyna</i>	<i>Corylus avellana</i>	<i>Acer pseudoplatanus</i>	<i>Fraxinus excelsior</i>	<i>Quercus robur</i>	Others
Abbreviation	CRATMO	CORYAV	ACERPS	FRAXEX	QUERRO	-
Number (2016)	24	65	542	81	34	104
Number (2022)	23	64	535	78	33	98
Matched number (2016 & 2022)	23	64	535	78	33	98
<i>c</i> (g C/g biomass)	0.478	0.478	0.469	0.491	0.474	0.478
<i>ρ</i> (g/cm ³)	0.52	0.517	0.51	0.56	0.56	0.525

for each DBH group: individual counts, biomass carbon stocks, and mean absolute change of each forest structural attribute. These indicators help to assess the distribution of tree size, growth dynamics, and the contribution of different DBH groups to carbon stock.

2.7. Evaluation metrics

The dynamic changes in forest structural attributes and biomass carbon over the six-year period were evaluated using absolute change (AC), mean absolute change (MAC), and relative change (RC) metrics. AC is defined as the difference between the structural attribute value in 2022 and the corresponding value in 2016, representing the magnitude of variation in forest structural attributes. MAC is calculated as the absolute change magnitude divided by the corresponding number of trees. RC is calculated as the change in structural attributes from 2016 to 2022 relative to their values in 2016, thereby enabling comparability among trees of different sizes after standardizing the structural attributes. The calculation methods for these metrics are as follows:

$$\text{Absolute change (AC)} = M_{2022} - M_{2016} \tag{2}$$

$$\text{Mean absolute change (MAC)} = \frac{\sum_{i=1}^n (M_{2022} - M_{2016})}{n} \tag{3}$$

$$\text{Relative change (RC)} = \frac{M_{2022} - M_{2016}}{M_{2016}} \tag{4}$$

where M_y is the structural attribute value in year y , and n is the quantity of trees.

3. Results

3.1. Forest structure dynamics

The characteristic distributions of DBH and H attributes from Wytham Woods 2016 and 2022 are shown in Fig. 1. The DBH and H distributions of CRATMO and CORYAV were generally smaller and narrower compared to other species, with DBH ranging from 3 cm to 24 cm and H ranging from 2 m to 15 m. ACERPS exhibited a more evenly distributed DBH and H, with DBH ranging from 2 cm to 85 cm, except for the largest tree, which exceeded 120 cm, and H ranging from 2 m to 32 m. Additionally, ACERPS was the most abundant species, with 542 trees in 2016 and 535 trees in 2022, accounting for approximately 64.0 % of the total. The DBH and H distribution of FRAXEX were similar to those of ACERPS, but its population was only about 15.0 % of ACERPS. The QUERRO population is primarily composed of large trees, exhibiting a DBH between 40 cm and 105 cm, and heights ranging from 15 m to 25 m.

Over the six-year period from 2016 to 2022, 19 trees died, including seven ACERPS, four FRAXEX, one CRATMO, one CORYAV, and six trees from unidentified species. Stem density declined from 607 stems per hectare in 2016 to 594 stems per hectare in 2022. DBH group statistics

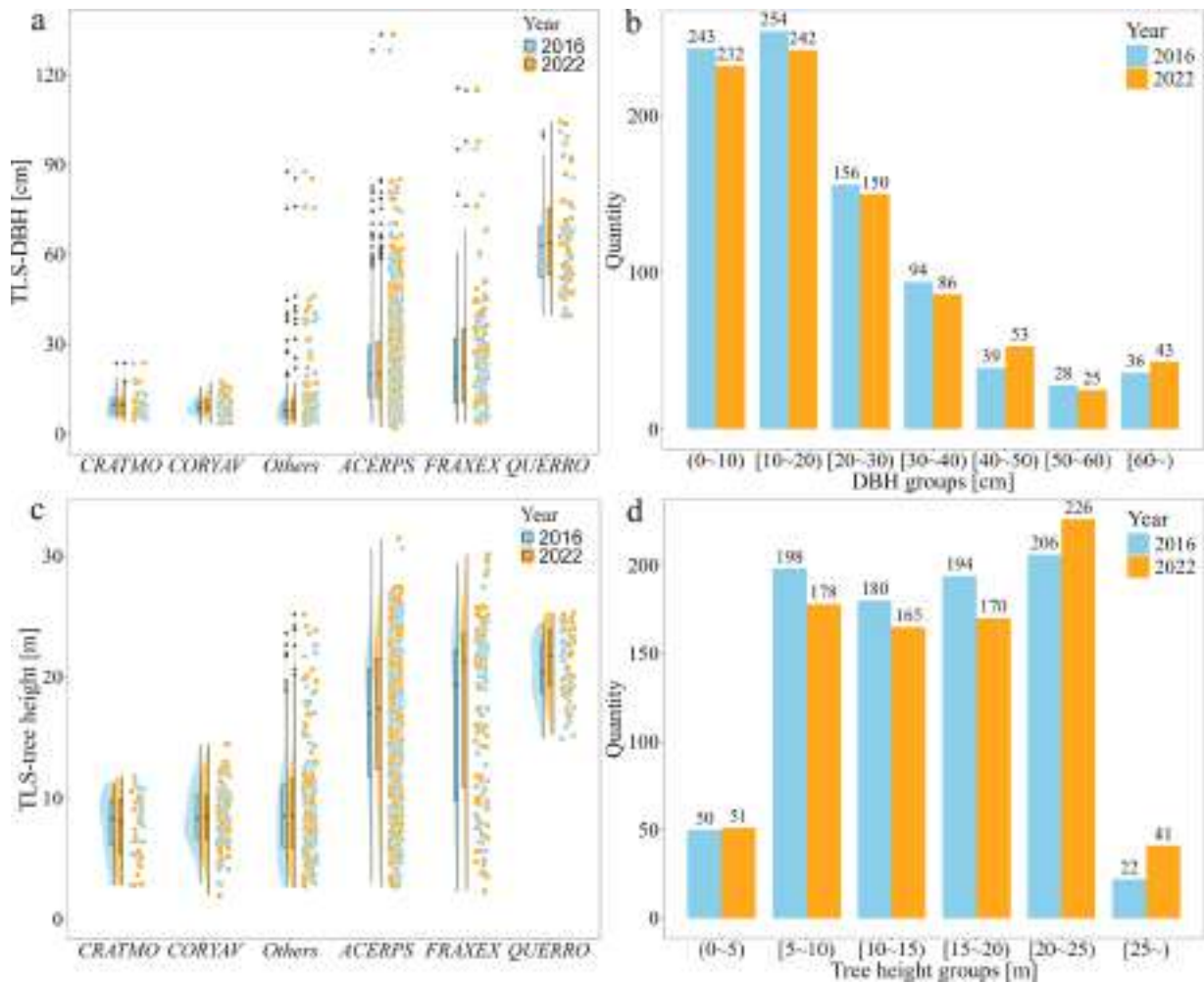


Fig. 1. Dataset characteristics of diameter at breast height (DBH) and tree height derived from terrestrial laser scanning (TLS) data. Panel a and c indicate the DBH and tree heights calculated from Wytham Woods 2016 and 2022 point clouds, respectively. Panel b and d indicate the quantity of trees in different DBH groups and tree height groups, respectively.

indicate that in 2016, 653 trees had a DBH of <30 cm, accounting for approximately 76.8 % of the total, which decreased to 75.1 % in 2022. Moreover, a decreasing trend in tree number was evident across most DBH groups, except for the 40–50 cm DBH group, which net gained 14 trees, and the over 60 cm DBH group, which increased by seven trees. The distribution of H was primarily concentrated between 5 m and 25 m, with 791 trees (approximately 91.5 %) in this range in 2016 and 739 trees (approximately 88.9 %) in 2022.

3.3.1. Comparison of TLS-derived and forest census

A total of 679 living trees were successfully matched between TLS point clouds and field forest census data in Wytham Woods for both 2016 and 2022. Comparison between the TLS-derived DBH and corresponding field measurements is shown in Fig. 2. The TLS-derived DBH values showed strong agreement with field-measured DBH values, with coefficients of determination (R^2) of 0.988 and 0.989 for 2016 and 2022, respectively. Furthermore, the root mean square error (RMSE) for both years was 2.0 cm, indicating a stable performance of the DBH estimation algorithm and an assessment uncertainty of approximately ± 2.0 cm.

3.3.2. Tree-level structural attribute change

Based on 831 matched trees, the temporal changes (species-level groups) at tree-level structural attributes over the six-year period can be found in Fig. 3.

Not all trees have achieved a consistently positive growth in DBH (approximately 60.2 %) over the six-year period as measured by TLS, with 331 trees (approximately 39.8 %) exhibiting reductions. Among the 831 trees, the DBH AC values of 766 individuals (approximately 92.2 %) fell within the range of -3 cm to 3 cm (Fig. 3a). Taking into account the uncertainty of the DBH estimation, 138 trees (13 with negative and 125 with positive changes), representing 16.6 % of 831 matched trees, exhibited DBH AC exceeding 2.0 cm and were considered to have undergone substantial structural change. Although DBH decreases were observed across different species, obvious interspecific differences did exist among them (Fig. 3a). Apart from the CRATMO, the mean and median values of DBH AC were positive for other species, indicating that most trees experienced positive DBH growth. Notably, reductions in field-measured DBH were also observed, accounting for approximately 11.1 % of 679 matched trees. A comparison between TLS-derived DBH AC and those obtained from field forest census is presented in Appendix Fig. A2. The RMSE between TLS-derived DBH change values and field-measured DBH change values was 1.2 cm.

As expected, the majority of trees (approximately 76.0 %) have

exhibited positive height growth over the six-year period. However, a few trees experienced decreases in height, with two individuals showing a reduction of >6 m, which have been annotated with A and B in Fig. 3b. The height reductions of the two trees were caused by bole snapping (A) and treefall (B), respectively (Fig. 4). Similarly, the tree annotated as C and the FRAXEX individual with the greatest height reduction also experienced bole snapping and treefall, respectively. Notably, absolute changes (ACs) in H are strongly associated with tree size. For instance, most individuals of CRATMO and CORYAV, which are generally smaller than other species (Fig. 1), had median absolute height changes close to zero, and their MACs were negative, indicating that nearly half of the trees from these two species experienced height reductions. In contrast, ACERPS, FRAXEX, and QUERRO showed positive median and mean values of height AC, indicating a general trend of significant height increase in these species over the past six years.

Approximately 64.7 % and 60.5 % of trees exhibited positive changes in CPA and CV, respectively. No substantial increases in CPA and CV were observed for the species with larger tree size (e.g. QUERRO) compared to others (Fig. 3c and 3d). On the contrary, although all QUERRO individuals were evidently larger than CORYAV trees (Fig. 1), the MAC values for CPA and CV in QUERRO were considerably lower than those in CORYAV. Notably, CORYAV exhibited the maximum MAC values for both CPA and CV among all species, indicating a more pronounced overall positive growth trend in these crown metrics. Some trees exhibited decreases or increases in CPA or CV. One ACERPS tree D showed the greatest CPA absolute reduction, losing approximately 33 m² (-33.0 %) compared to 2016 (Fig. 4). This was primarily attributed to branch breakage and its height being significantly lower than surrounding trees, resulting in weakly competitive ability to grow (Fig. 5). A QUERRO tree F had the largest absolute increase in CPA, gaining approximately 38 m² (16.6 %) since 2016 (Fig. 4). This was mainly attributed to its height dominance over surrounding trees and the death and subsequent fall of a large neighbouring tree, which released additional space for crown expansion (Fig. 5). Another QUERRO individual L exhibited the greatest CV absolute reduction of approximately 445 m³ (-40.6 %) primarily caused by major branch breakage and loss within the crown (Figs. 4 and 5). Similar causes were identified for most of the other trees showing substantial reductions in CPA and CV.

In the case of the calculated volume from QSMs, only about half of the trees (50.5 %) showed an increase compared to 2016. Except for FRAXEX, which had a MAC value of 0.2 m³, volume growth across other species was not remarkable. Trees with the large absolute decreases in V also exhibited marked declines in CPA or CV, caused by substantial

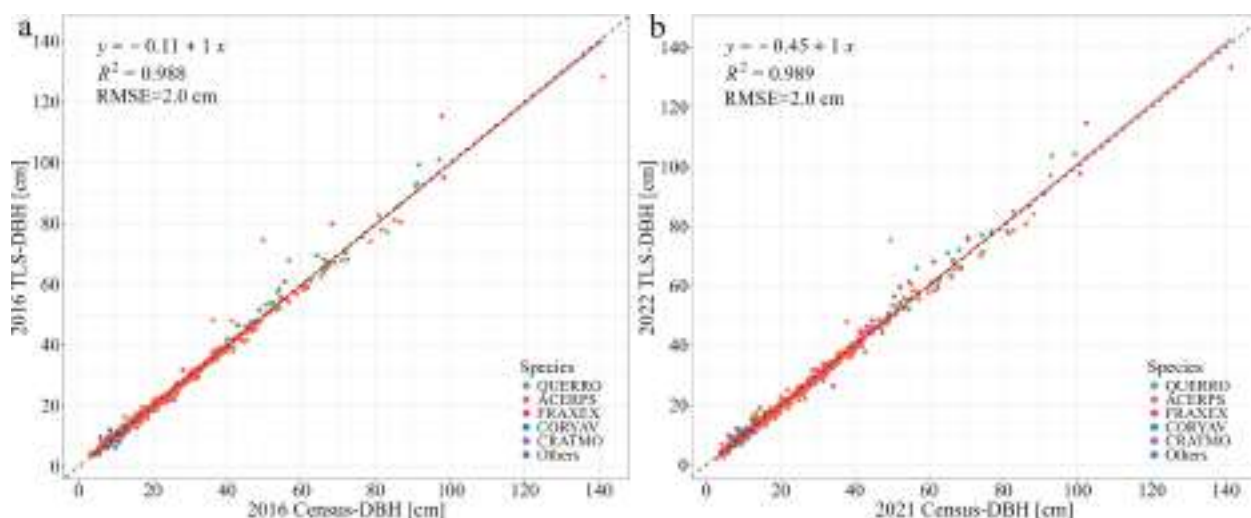


Fig. 2. Comparison of TLS-derived DBH and field measured DBH values. a and b represent the comparison of DBH in two survey years. TLS: terrestrial laser scanning, DBH: diameter at breast height, RMSE: root mean square error.

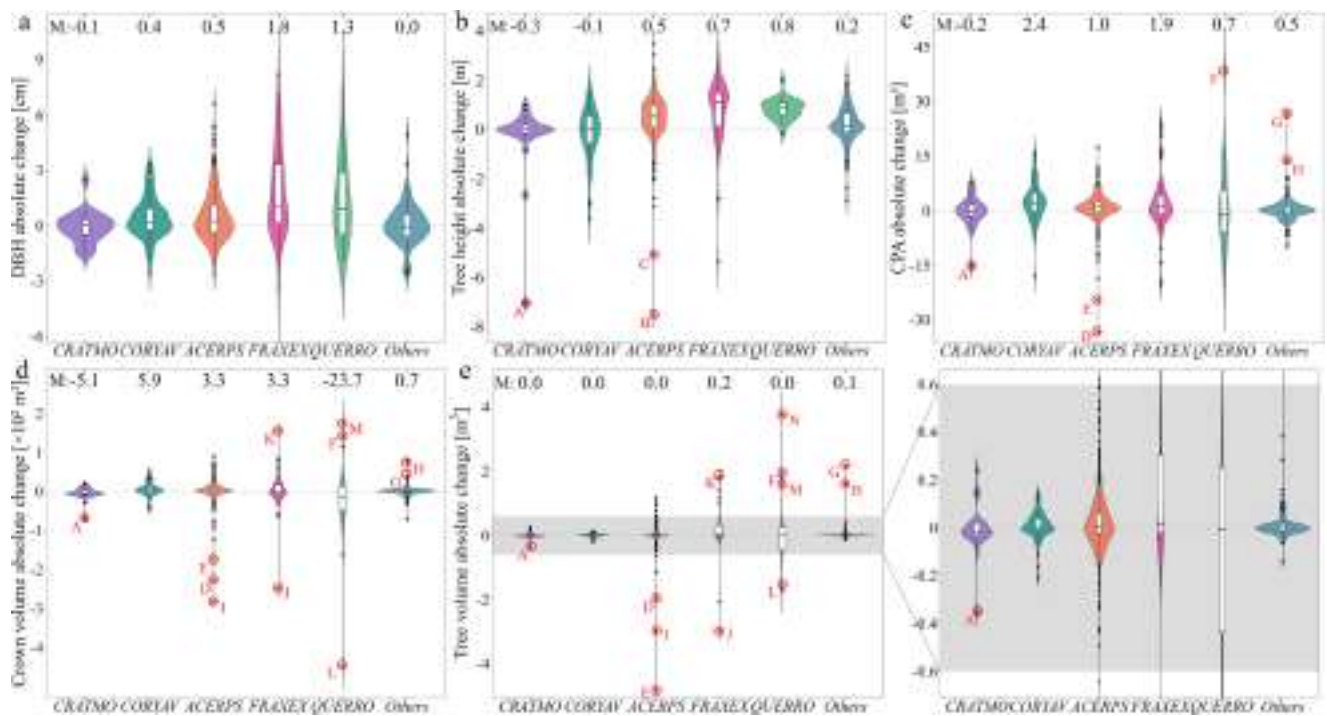


Fig. 3. Temporal variations in tree-level structural attributes of different tree species from 2016 to 2022. Panels a, b, c, d, e represent the absolute changes over six years in the structural attributes: diameter at breast height (DBH), tree height, crown projection area (CPA), crown volume, and aboveground tree volume, respectively. ‘M’ represents the mean absolute change in structural attributes for different tree species. Red letters mark trees with large variations in structural attributes.

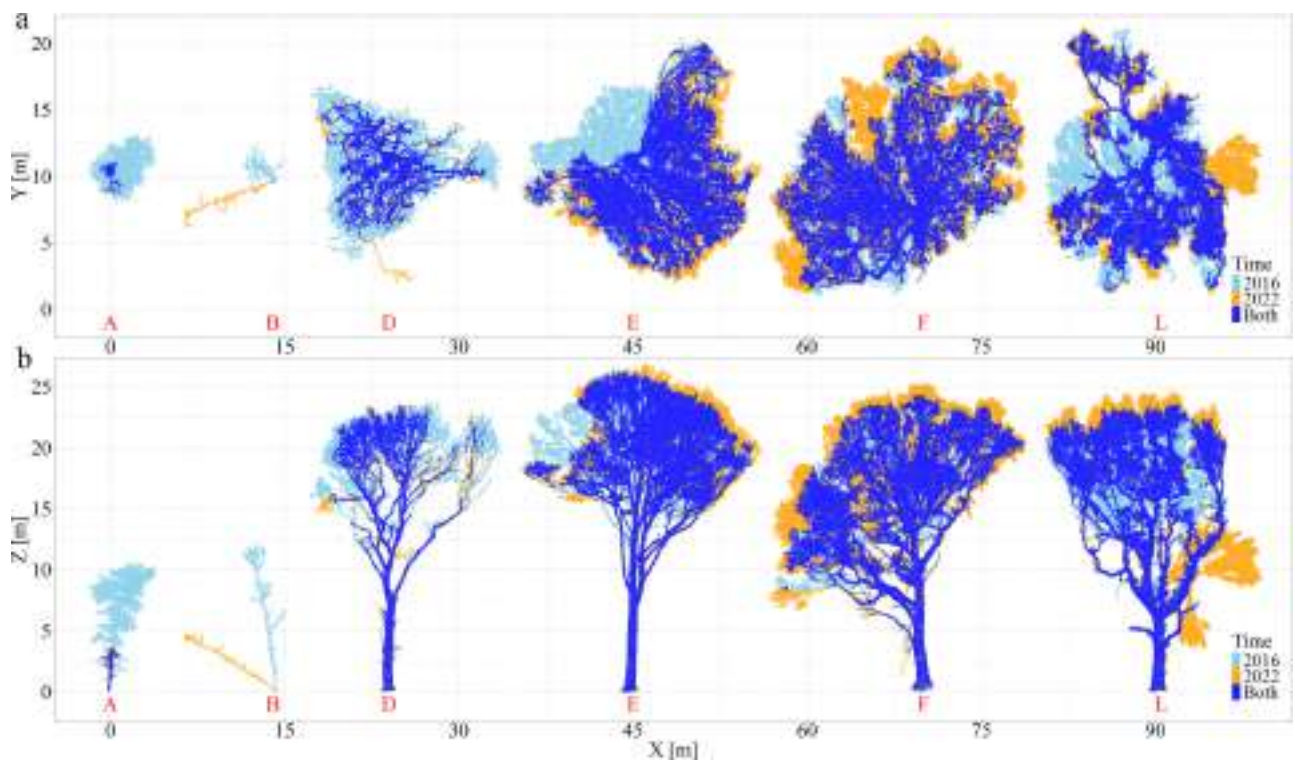


Fig. 4. Trees exhibiting substantial structural attribute changes (absolute change) between 2016 and 2022. The trees marked with red letters correspond to those identified in Fig. 3 as having undergone substantial changes in structural attributes.

branch loss. Manual inspection of point clouds for the tree with the largest volume reduction (tree E), as well as other trees with volume loss, confirmed that the decrease in V was primarily due to branch loss

(Figs. 4 and 5). Furthermore, the increase in tree volume was mainly driven by crown expansion, followed by trunk growth.

The results of the relative change (RC) at the tree-level structural

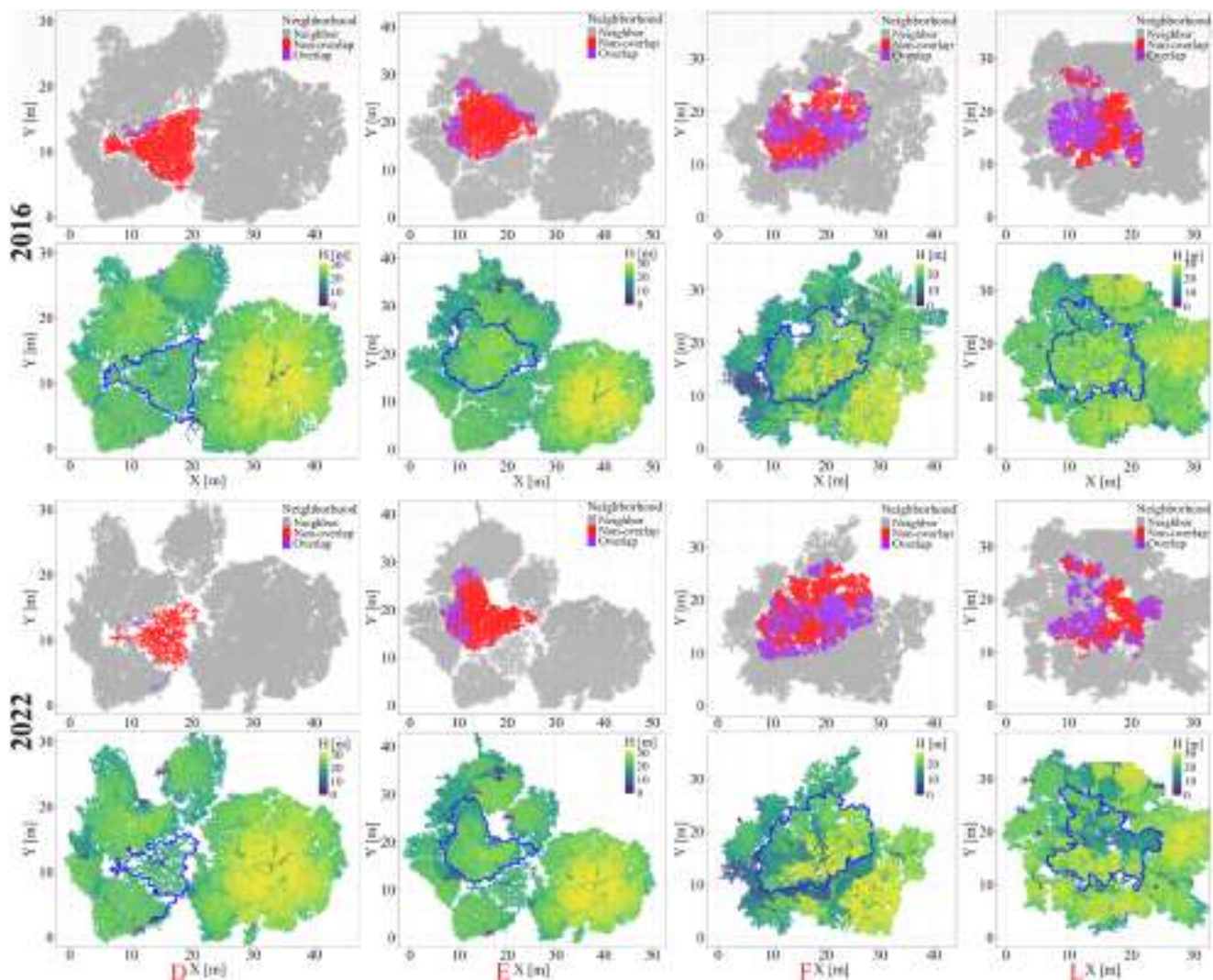


Fig. 5. Temporal dynamics of surrounding tree structures around specific trees from 2016 to 2022. The trees marked with red letters correspond to those identified in Fig. 4 as having undergone substantial changes in structural attributes. Each column represents the spatial distribution of the surroundings of the same tree in 2016 and 2022. H: tree height.

attributes indicate no notable differences among different species (Fig. 6). Trees exhibiting larger absolute values of the structural attribute RC are observed to have a DBH of <10 cm. Trees with DBH-associated RC values exceeding 0.4 are all individuals with DBH around 5 cm, particularly the tree with the highest RC (tree O), whose DBH measured 2.9 cm in 2016 and 5.1 cm in 2022 (Fig. 7). Two trees with abnormally decreased height RC have already been identified in Fig. 3: tree A (−65.6 %) and tree B (−61.4 %), while another tree Q (−55.4 %) with a reduced RC is attributed to branch loss (Fig. 7). One CORYAV individual P exhibits the largest increase in height RC (34.2 %), along with noticeable RC increases in CPA (222.4 %), CV (445.8 %), and V (275.4 %), primarily due to crown growth (Fig. 7). Furthermore, trees displaying notable relative increases in CPA (F, G, H, K, and J) also exhibit marked corresponding relative increases in CV and V (Fig. 6).

The temporal dynamics of tree-level structural attributes over the six-year period, categorized by DBH groups, are shown in Fig. 8. The MAC and median values of different structural attributes generally exhibit an initial increase followed by a slight decreasing trend with increasing DBH. Trees with DBH <20 cm have smaller MAC values for both DBH and H compared to other DBH groups, and have noticeably more trees with negative AC values than other DBH groups. The MAC values of DBH increase across the DBH groups of 10–20 cm (0.1 cm), 20–30 cm (0.7 cm), and 30–40 cm (1.6 cm), and then tend to stabilize

(1.7–2.0 cm). Similarly, the MAC values of H increase in the 10–20 cm (0.3 cm) and 20–30 cm (0.8 cm) DBH groups, and then stabilize (0.8–1.0 cm). For CPA, CV, and V, MAC values show an increasing trend with DBH, reaching their maximum in the 30–40 cm and 40–50 cm DBH groups, followed by a decreasing trend as DBH further increases. Notably, in the DBH groups over 60 cm, both the MAC and median values for CPA, CV, and V are all below zero.

The median RC values of tree-level structural attributes across DBH groups, exhibit a distribution pattern similar to that of the median AC values, characterized by an initial increase followed by a slight decrease with increasing DBH (Fig. 9). A broader range of RC values and more frequent outliers for structural attributes are predominantly concentrated in the 0–10 cm DBH group. This can be attributed to small trees inherently having lower absolute structural attribute values, and thus, the same magnitude of measurement error results in disproportionately larger RC values for these individuals.

3.3.3. Plot-level structural attribute change

The canopy cover of the 1.4 ha study area in 2016 and 2022 is shown in Fig. 10. Some canopy gaps present in 2016 were filled by forest growth by 2022 (green areas), while spaces previously occupied by standing dead trees in 2016 were released due to treefalls by 2022 (red areas), thereby creating new space for the expansion of surrounding

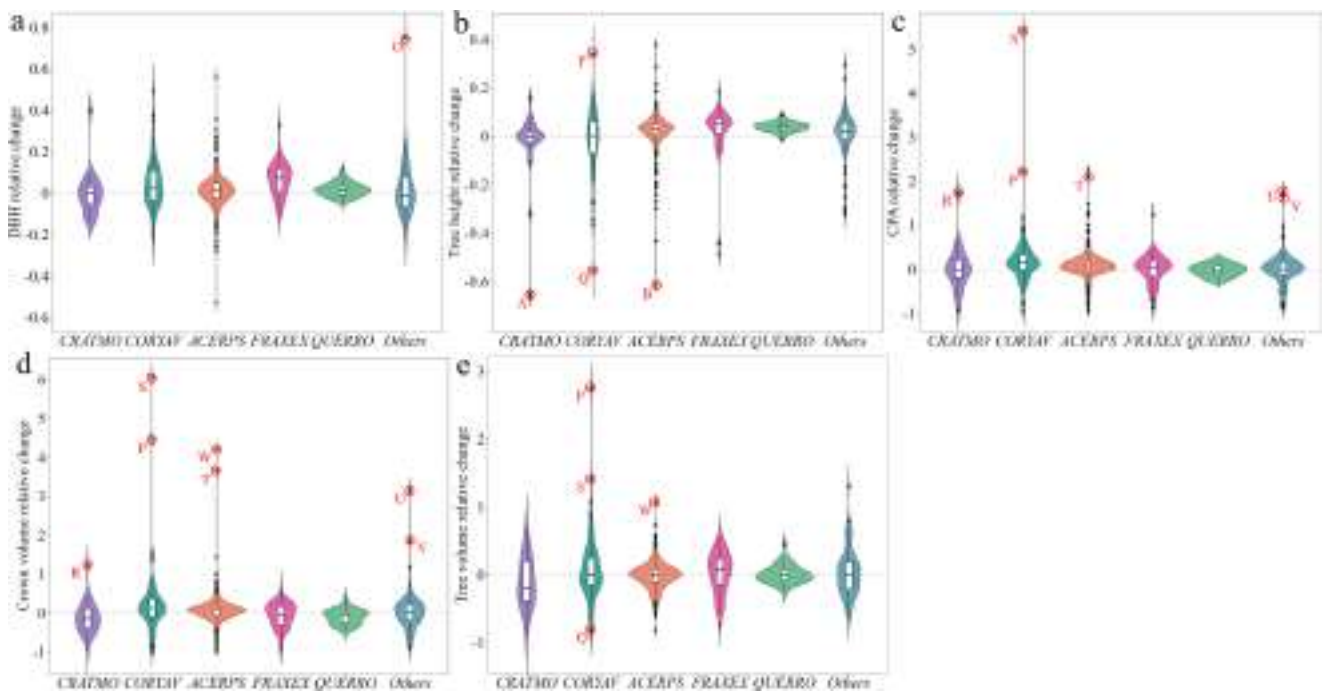


Fig. 6. Relative growth variations in tree-level structural attributes of different tree species from 2016 to 2022. Panels a, b, c, d, e represent the relative changes over six years in the structural attributes: diameter at breast height (DBH), tree height, crown projection area (CPA), crown volume, and tree volume, respectively. Red letters mark trees with large variations in structural attributes.

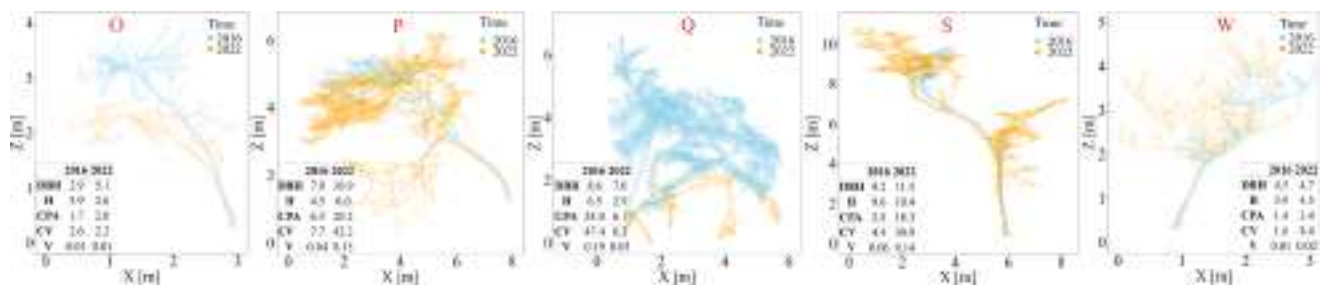


Fig. 7. Point clouds of trees exhibiting pronounced relative changes between 2016 and 2022. The trees marked with red letters correspond to those identified in Fig. 6 as having undergone anomalous relative changes in structural attributes. DBH: diameter at breast height, [cm]; H: tree height [m]; CPA: crown projection area, [m²]; CV: crown volume, [m³]; V: aboveground tree volume, [m³].

crowns.

At the plot level, the mean per-tree AC in forest structural attributes over the six-year period are as follows: DBH increased by 0.8 cm, H by 0.6 m, CPA by 1.3 m², CV by 3.3 m³, and V by 0.04 m³. The average per-tree AC values in structural attributes from 2016 to 2022 for different tree species are presented in Appendix Fig. A3. All structural attributes of CRATMO exhibit varying degrees of decline, with H showing the largest absolute decrease among all species, averaging -0.3 m. For CORYAV, except for a slight reduction in average H compared to 2016, all other structural attributes increased, with CPA and CV displaying the largest absolute increases across species, at 2.4 m² and 5.9 m³, respectively. ACERPS exhibits positive growth in structural attributes except for a slight decrease in average volume (-0.02 m³). In the case of FRAXEX, all structural attributes increased, with DBH, H, and volume increasing by 1.8 cm, 1.1 m, and 0.21 m³, respectively. With regards to QUERRO, the most distinct decline is observed in CV, primarily due to the substantial loss of branches, while the other structural attributes show positive growth.

BA, H, CPA, DBHCV, and V at plot-level all increased over the six-year period, with respective increases of 1.8 m²/ha, 128.9 m/ha, 411.9 m²/ha, 1.5 m/ha, 181.7 m³/ha, and 7.9 m³/ha (Fig. 11). ACERPS

demonstrates the highest proportion and greatest absolute increase in BA, H, CPA, DBH, and CV among species, primarily due to its dominance and most abundant species within the study area. FRAXEX exhibits an overall positive growth trend across all forest structural attributes, whereas CRATMO shows a slight decrease in all attributes. CORYAV shows a slight increase in most attributes, with the exception of a slight decrease in H. QUERRO has achieved slight increases in BA, H and CPA, while experiencing negative growth in DBH, CV, and V.

3.2. Aboveground biomass carbon dynamics

The total AGBC stock of the 1.4 ha study area remains stable over the six-year period, with values of 269.93 Mg C in 2016 and 272.98 Mg C in 2022, with a net carbon gain of 2.18 Mg C/ha (Fig. 12). The gross carbon gain in living trees (3.05 Mg C) over the six-year period is generally consistent with the carbon stock absolute increase of FRAXEX trees (3.11 Mg C). Although the overall DBH, H, CPA, and CV structural attributes of ACERPS and QUERRO exhibited positive trends, their overall carbon stocks did not increase accordingly. Trees of CORYAV and CRATMO have smaller tree sizes and are less abundant than those of other species, resulting in lower carbon stocks and smaller changes in absolute carbon

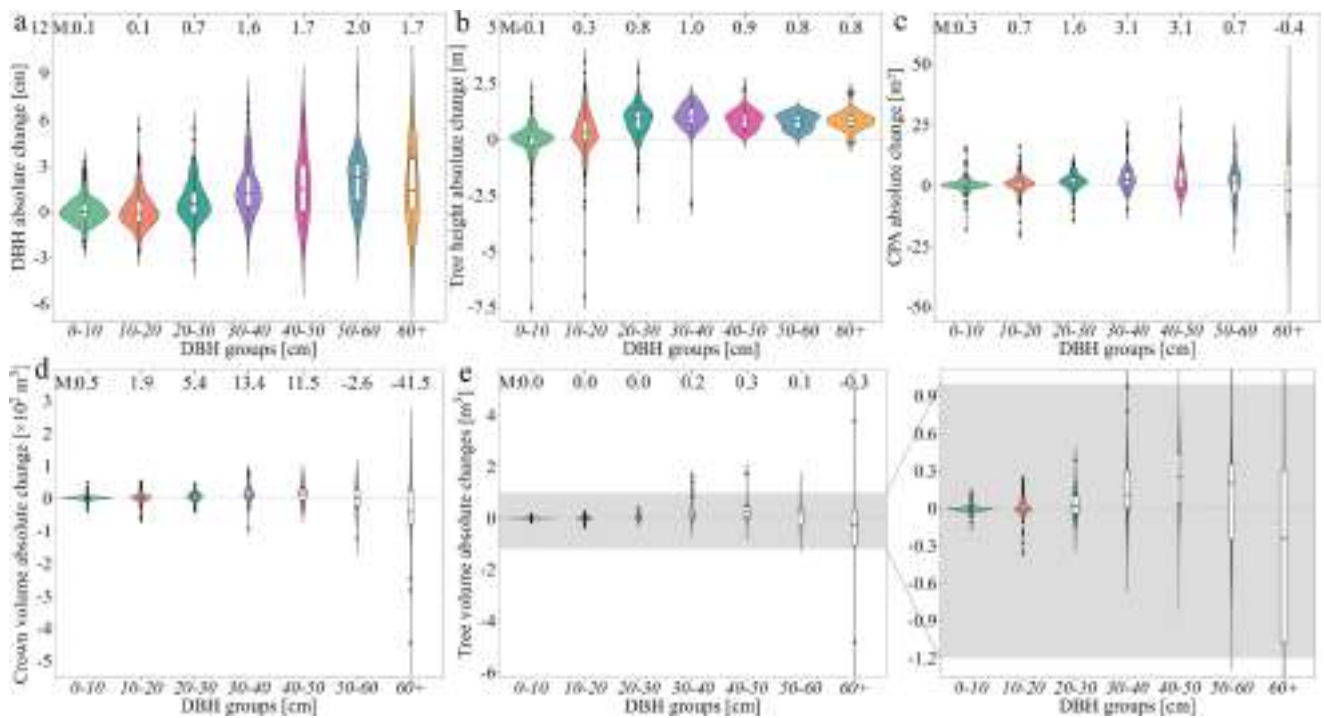


Fig. 8. Temporal dynamic changes in tree-level structural attributes of different diameter at breast height (DBH) groups from 2016 to 2022. Panels a, b, c, d, e represent the absolute changes over six years in the structural attributes: DBH, tree height, crown projection area (CPA), crown volume, and aboveground tree volume, respectively. ‘M’ represents the mean absolute change in structural attributes for different DBH groups.

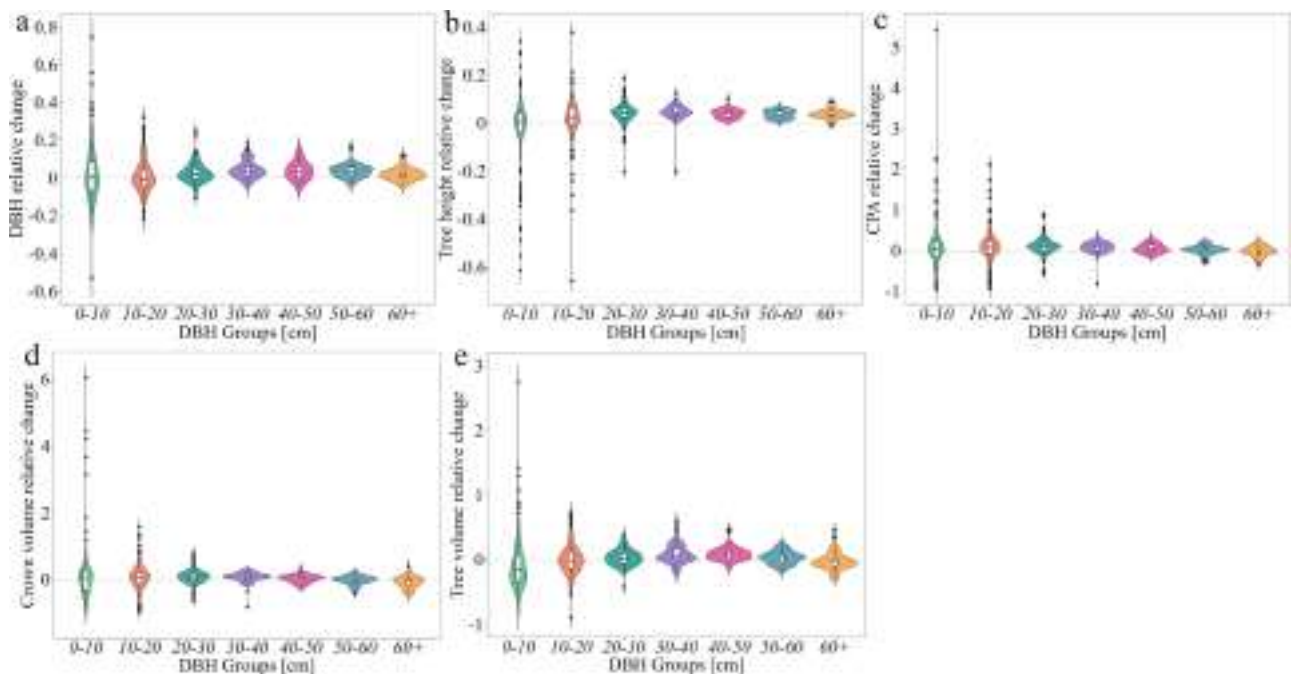


Fig. 9. Relative growth variations in tree-level structural attributes across different diameter at breast height (DBH) groups from 2016 to 2022. Panels a, b, c, d, e represent the relative changes over six years in the structural attributes: DBH, tree height, crown projection area (CPA), crown volume, and aboveground tree volume, respectively.

dynamics over time. The carbon stock of unidentified species increased by 1.08 Mg C (10.4 %). In contrast, the carbon stock of standing dead trees declined from 4.70 Mg C in 2016 to 1.86 Mg C in 2022. Correlation analysis between the AC in AGBC stock and the AC values of carbon stock in branch and trunk components reveals that AGBC dynamics are more strongly associated with changes in branch carbon (Branch: $R^2 =$

0.931, Trunk: $R^2 = 0.169$, Fig. 13).

For carbon dynamic changes within DBH groups, the 40–50 cm DBH group has the highest carbon gain (11.02 Mg C, 39.3 %) over the six-year period, followed by the DBH group over 60 cm (6.47 Mg C, 5.9 %), while the remaining DBH groups experienced carbon loss (Fig. 12). The 30–40 cm DBH group experienced the greatest carbon loss from 2016 to 2022

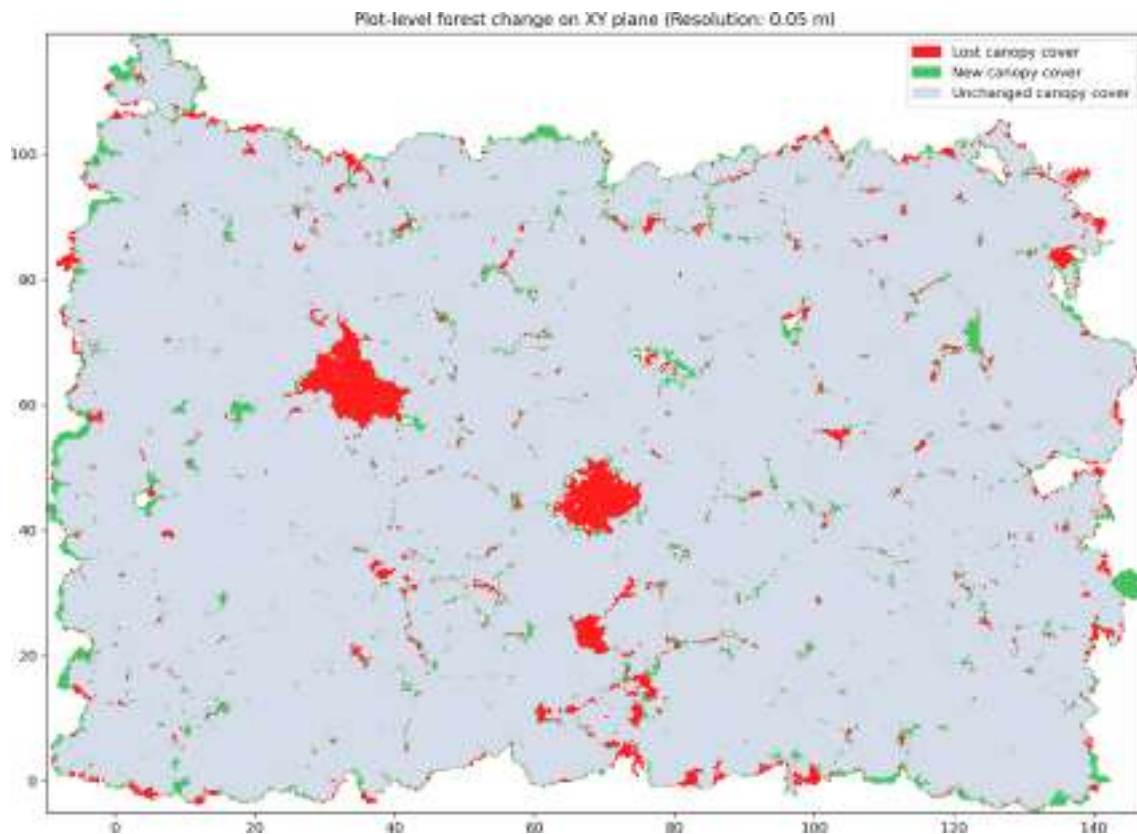


Fig. 10. Raster map showing plot-level canopy cover dynamics between 2016 and 2022. Lost canopy cover represents areas with canopy cover in 2016 but no cover in 2022. New canopy cover represents the area newly covered by canopy in 2022. Unchanged canopy cover represents the area covered by canopy in both 2016 and 2022.

(-6.12 Mg C, -14.1 %), followed by the 50–60 cm DBH group (-4.93 Mg C, -14.0 %). The remaining three DBH groups with diameters below 30 cm collectively lost a total of 3.4 Mg C of carbon. Trees in the DBH group greater than 60 cm accounted for 40.7 % and 42.7 % of the total AGBC stock in the 1.4 ha study area in 2016 and 2022, respectively. The carbon stock proportion of the 40–50 cm DBH group increased from 10.4 % in 2016 to 14.3 % in 2022. In contrast, the proportions of the 30–40 cm and 50–60 cm DBH groups decreased by 2.4 % and 2.0 %, respectively, compared to their 2016 levels.

4. Discussion

In this study, we demonstrated that the integration of bi-temporal TLS data with QSM enables quantification of forest structural attributes and AGBC dynamics at both the individual tree and plot scales, highlighting the application potential of multi-temporal TLS in forest monitoring and for tracking forest structural dynamics.

4.1. Forest structural attribute change

Our results demonstrate that, based on bi-temporal TLS data, the majority of trees exhibited positive growth at the individual-tree level in terms of DBH (60.2 %), H (75.8 %), CPA (64.7 %), CV (60.5 %), and V (50.5 %), over the six-year period from 2016 to 2022. Nevertheless, negative absolute change values of these structural attributes were also observed, pointing at net size reductions over the studied period. Similarly, a study on boreal forests by Yrttimaa et al. (2020) reported that a considerable proportion of trees showed negative growth in DBH, BA, and H over a five-year period from 2014 to 2019, based on both TLS data and field inventory measurements. In terms of theoretical tree growth patterns, these structural attributes are expected to show consistent

positive increments over time (Pretzsch, 2010; Zhao et al., 2018). However, due to the frequent occurrence of natural disturbances such as ash dieback, storms, droughts, and heatwaves at Wytham Woods during the six-year period (Buras et al., 2020; Knutzen et al., 2025), some trees experienced mortality, severe structural damage, or growth limitations (Figs. 4 and 5). Previous studies have confirmed that disturbances are among the most influential drivers of forest structural dynamics, often exerting negative impacts on structural attribute development (Seidl et al., 2017; Thom et al., 2022). Additionally, although TLS systems capture highly detailed structural information with millimeter-level point accuracy—providing more accurate and comprehensive structural attribute assessments than other LiDAR platforms such as mobile, UAV-based, or airborne laser scanning—potential factors including point cloud density, scanning distance, registration errors, occlusion, wind, and instrument-related errors can still introduce errors in the estimation of forest structural attributes (Calders et al., 2015; Demol et al., 2022; Liang et al., 2018; Wilkes et al., 2017). Another major source of uncertainty stems from the structural attribute extraction algorithms (Bogdanovich et al., 2021; Luoma et al., 2021; Raunonen et al., 2013; Terryn et al., 2023). For example, comparison with field-based DBH census data revealed that the RMSE of TLS-derived DBH was 2.0 cm for both survey years in this study (Fig. 2), which is in close agreement with the RMSE of 2.3 cm reported by Terryn et al. (2023). It is also worth noting that, beyond these factors, species-specific characteristics may contribute to observed negative AC values in DBH. For instance, stem bark peeling and renewal associated with tree aging in species such as FRAXEX and ACERPS can lead to apparent reductions in DBH measurements over time. In addition, our results showed that the MAC (measurement uncertainty) in DBH increased considerably with increasing DBH for trees within the 0–60 cm DBH groups. This pattern is consistent with the findings of Terryn et al. (2022), who reported that



Fig. 11. The distribution characteristics and changes (absolute change) in basal area (BA), tree height (H), crown projection area (CPA), diameter at breast height (DBH), crown volume (CV), and aboveground tree volume (V) across different tree species from 2016 to 2022.

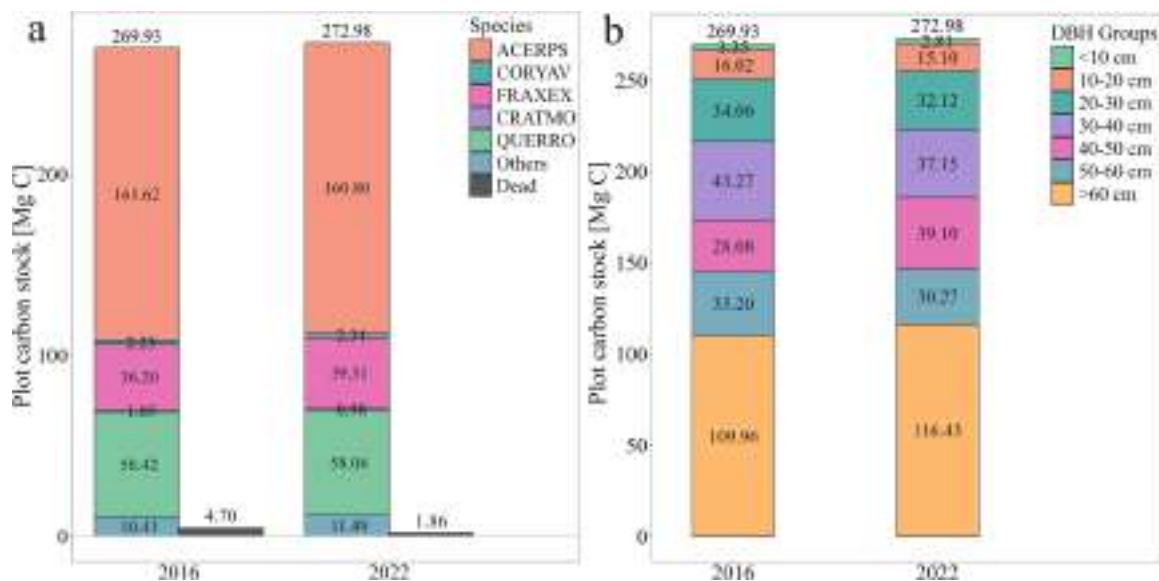


Fig. 12. The distributions of aboveground biomass carbon within the study area in 2016 and 2022. ‘a’ represents the carbon stock distribution of different tree species. ‘Dead’ refers to the standing dead trees. ‘b’ represents the carbon stock distribution across different DBH groups.

larger DBH values (DBH range 10–88 cm) are associated with greater measurement uncertainties. Furthermore, field census data also showed that approximately 11.1% of trees exhibited negative DBH AC values between 2016 and 2021, which could be attributed to inconsistencies in field crews, measurement positions, or other operational factors Appendix Fig. A2).

The observed temporal dynamics in forest structures can be attributed to factors such as species-specific traits, species abundance imbalances, crown competition, and tree size variability (Astigarraga et al., 2025; Fu et al., 2021; Griebel et al., 2015; Luoma et al., 2021; Martin-Ducup et al., 2017; Yrttimaa et al., 2020). From 1974 to 2012, the basal area of several tree species in Wytham Woods, including ACERPS,

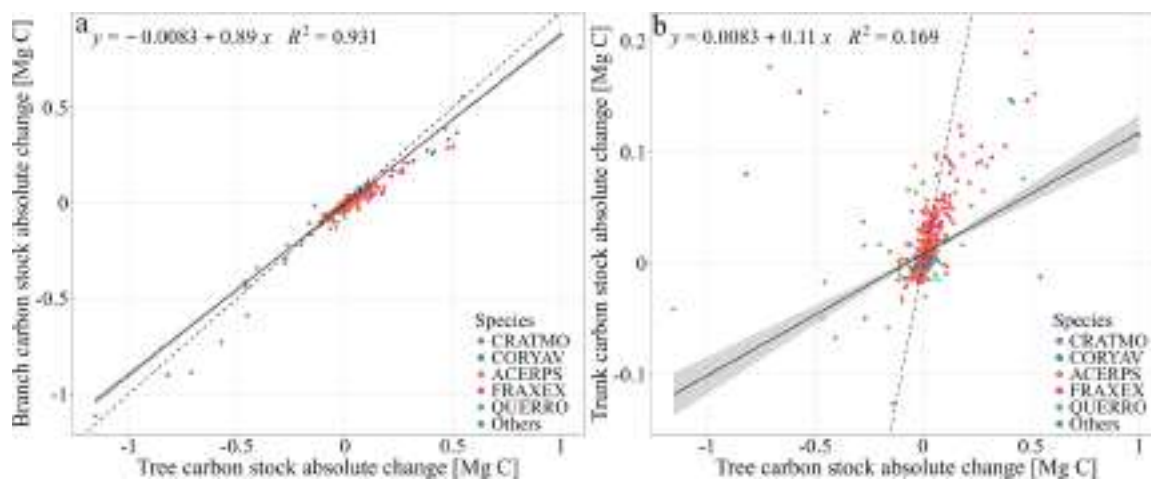


Fig. 13. The correlation between the absolute change in aboveground carbon stock and the absolute changes in branch and trunk carbon stock.

FRAXEX, and QUERRO, had seen a steady increase, which had resulted in the majority of young, small trees transforming to mature, large trees, with the modal diameter class having shifted from 11–20 cm to 30–40 cm (Kirby et al., 2014). These larger trees dominate the competition for sunlight, water, nutrients, and space, thereby effectively promoting growth. In contrast, suppressed understory trees, such as CRATMO and CORYAV, characterized by DBH < 24 cm and height < 15 m, experience growth limitations due to competitive disadvantage (Fig. 3) (Coomes and Allen, 2007; Martin-Ducup et al., 2020). Coomes and Allen (2007) further demonstrated that light competition significantly limits the growth of small trees, while nutrient competition affects trees across all size classes.

As a result of natural disturbances, some trees died and fell to the ground between 2016 and 2022, which created canopy gaps for the lateral expansion of adjacent tree crowns (Fig. 10). At the same time, some canopy gaps that existed in 2016 were gradually filled in by the growth of neighboring tree crowns. Martin-Ducup et al. (2017) quantified crown expansion using four crown-derived metrics and found that, two years after the release from crown competition, a large proportion of crown area exhibited considerable downward space reoccupation. Their analysis further revealed substantial structural changes in both the vertical and horizontal dimensions of the crown. Their findings provide valuable insights into the mechanisms of crown expansion and how trees reoccupy space released by both localized and large-scale disturbances. Furthermore, Wang et al. (2022) developed the PlantMove tool to reconstruct patterns of crown expansion movement from multi-temporal point cloud data, thereby revealing the temporal dynamics of crown expansion and offering a valuable tool for interpreting spatial patterns of crown dynamics.

4.2. Aboveground biomass carbon dynamics

Our results revealed that the total AGBC in the study area remained stable over the past six years (Fig. 12a), with a net carbon gain of 2.18 Mg C/ha (AGB about 4.42 Mg/ha) during this period. Furthermore, from a fine-scale, tree-level perspective, our study captured the 3D structural changes of individual trees over time and demonstrated how structural dynamics at the tree level underpin the plot-level stability of AGBC through a compensatory mechanism of carbon loss and gain. In contrast, single-time-point TLS data can only provide a static assessment of forest structure and carbon stock at a certain moment, without capturing the temporal dynamics of AGBC at the individual tree level. Bi-temporal TLS point clouds clearly revealed structural changes, including branch loss and growth in individual trees, yielding critical insights into the drivers of AGBC dynamics. Srinivasan et al. (2014) also assessed tree-level AGB changes over a three-year period using

multi-temporal TLS data from a pine–hardwood mixed forest. However, their approach primarily relied on developing biomass models based on TLS-derived parameters to estimate AGB changes, without directly linking structural changes of individual trees to the observed biomass dynamics.

The species-specific dynamics of AGBC over the past six years show that, overall, FRAXEX exhibited a noticeable carbon gain, while other species maintained relatively stable AGBC levels (Fig. 12). This can be largely attributed to the faster growth rate, higher water and nutrient use efficiency, and lower vulnerability to natural disturbances of FRAXEX compared to the other species present in the study area. These advantages enabled this species to sustain favorable growth even though the study area experienced multiple disturbance events between 2016 and 2022. Consistent with this, the structural attributes of FRAXEX, including DBH, H, CPA, CV, and V, also showed greater absolute increases than those of other species (Fig. 3). Notably, although ash dieback was first detected at Wytham Woods in 2017, the disease remained in its early stages through 2022, without triggering large-scale mortality of FRAXEX individuals. However, with the anticipated spread of ash dieback in the coming years, a substantial increase in tree mortality and a reduction in growth rates are expected (Kirby et al., 2014). In contrast, CORYAV and CRATMO are typical understory species whose growth is inherently limited due to their structural characteristics and competitive disadvantages in terms of space occupancy, resulting in relatively stable AGBC over time. The reason for the insignificant changes in ACERPS and QUERRO is primarily explained by structural changes such as branch loss or death or tree mortality observed in some individuals of these species.

In this study, trees with a DBH greater than 60 cm, accounting for approximately 5 % of the total tree population, contributed >40 % of the AGBC and were responsible for a carbon gain of 6.47 Mg C between 2016 and 2022 (Fig. 12), as also reported by Calders et al. (2022). Furthermore, a global analysis of 25 plots from different regions by Piponiot et al. (2022) also confirmed that large trees (DBH ≥ 60 cm) contributed a large fraction to all biomass stocks and fluxes, whereas small trees (DBH < 10 cm) typically contributed <15 % of total biomass (small trees contributed only about 1 % in this study to the total plot-scale AGBC). Changes in AGBC across DBH groups were not only associated with structural shifts in individual trees but also closely linked to transitions of trees between DBH groups. For example, 21 trees were classified in the 30–40 cm DBH group in 2016 but had grown into the 40–50 cm DBH group by 2022. This transition explains the increase in AGBC observed in the 40–50 cm DBH group, accompanied by the decline in the 30–40 cm DBH group. Furthermore, by the analysis of carbon stock in both crowns and trunks, we found that changes in crown carbon exhibited a stronger correlation with AGBC dynamics than trunk

carbon changes (Fig. 13), which highlights the dominant role of crown and its dynamics in driving AGBC changes.

The uncertainty associated with assessing AGBC dynamics using TLS should not be ignored, including those arising from instrument accuracy, sampling resolution, workflow design, data processing and modelling approaches. Previous studies have demonstrated that traditional allometric models tend to significantly underestimate AGB, particularly for large trees (although in this study, field inventory data corresponding to each TLS campaign were obtained, they were not used to estimate AGB via allometric models) (Calders et al. 2022; Moeys et al. 2025). In contrast, the TLS-QSM approach has been shown to slightly overestimate AGB, typically within 20 % and particularly for smaller branches (Calders et al. 2015; Chen et al. 2025; Cooper, 2026, unpublished results; Demol et al. 2022). In this study, we selected TreeQSM (v2.0) as the single-tree QSM reconstruction algorithm. Following the optimization procedure described by Calders et al. (2015, 2018), we determined the optimal parameter set for each tree. We generated ten QSMs using the selected parameter set and adopted their mean values as the final model result to further reduce reconstruction uncertainty. Another potential source of error arises from species-specific wood density and carbon conversion factors. Given that different tree components exhibit varying wood densities and carbon content, these differences may introduce additional uncertainties into the AGBC estimations.

4.3. Limitations and prospects

In this study, we focused on quantifying forest structure and AGBC dynamics in a temperate, mature secondary forest using bi-temporal TLS data, and interpreted AGBC dynamics in terms of changes in forest structure. Forest structural dynamics were quantified at both the individual tree and plot scales by extracting structural attributes. However, detailed spatial changes in crown structure, such as how each tree crown has changed in the horizontal and vertical dimensions, the extent of these changes, and which branches within the crown experienced significant growth, loss, or spatial displacement over the six-year period, were not explicitly quantified. The development of automated algorithms capable of detecting and statistically characterizing such crown-level changes is urgently needed. In our study, a six-year interval between TLS acquisitions was sufficient to quantify the dynamics of forest structural attributes (DBH, tree height, CPA, CV, and aboveground volume) and AGBC. The appropriate minimal temporal interval for measuring structure and carbon dynamics depends on various factors, such as the accuracy of the method used, the growth rate of the studied tree species, and the specific structural attributes of interest. Additionally, due to occlusion effects within the crown, point cloud data for upper crown areas were partially missing, potentially affecting the accuracy of extracted structural attributes and QSM reconstruction results (Calders et al. 2015; Demol et al. 2021). The integration of UAV-based LiDAR and TLS data has shown promising potential to overcome these limitations (Terry et al., 2022). Moreover, in assessing AGBC dynamics, only live trees were considered, while carbon changes associated with trees that died during the six-year period were not accounted for. Although we estimated the carbon stock of standing dead trees using the wood density values of living individuals, in reality, the wood density of dead trees is lower than that of their living counterparts. Consequently, this study did not analyze the carbon stock dynamics of dead trees. Since the carbon pool of dead trees also represents an important part of aboveground carbon dynamics, further investigation is warranted to improve our understanding of terrestrial carbon cycling. Besides dead trees, leaves, belowground tree components, and understory vegetation were also excluded from the AGBC assessment, as these components contribute only a small proportion of total terrestrial carbon pool and are challenging to quantify accurately. According to reports on Forest Biomass and Primary Productivity, leaf biomass accounts for approximately 1.7 % of the total tree biomass in North American temperate

forests, understory vegetation contributes <1 % of total vegetation biomass, and belowground biomass represents roughly 21 % of total tree biomass. Furthermore, beyond the temperate broadleaved forest investigated in this study, the application potential of multi-temporal TLS extends to other forest types, including boreal, tropical, and subtropical forests at different developmental stages (i.e., young, middle-aged, mature, and over-mature stands), as well as coniferous and mixed forests, where structural and carbon dynamics remain largely unexplored.

5. Conclusion

We demonstrated the use of bi-temporal TLS data to quantify and assess fine-scale dynamics of forest structure and AGBC at both the individual tree and plot levels. Overall, repeated TLS provides a precise approach for quantifying forest structural and AGBC dynamics in temperate mature secondary forests over a six-year period. Our study found that FRAXEX exhibited the largest structural growth among all species. Trees with anomalous relative changes in structural attributes were mainly small individuals, typically with DBH <10 cm. Moreover, when categorized by DBH groups (10 cm intervals), the mean absolute change and median values of different structural attributes generally exhibited an initial increase followed by a slight decreasing trend with increasing DBH. The total AGBC of the 1.4 ha study area remained stable over the six-year period, with a value of 269.93 Mg C in 2016 and 272.98 Mg C in 2022. The carbon gain of living trees within the study area is 3.05 Mg C over the six-year period. Trees with DBH greater than 60 cm contributed over 40 % of the total AGBC and accounted for a carbon gain of 6.47 Mg C over the six-year period. Another important finding of our study is that variations in crown carbon play a primary role in driving AGBC dynamics, indicating that conventional carbon inventories based solely on DBH (and height) may overlook substantial portions of the actual carbon dynamics. This study demonstrates the strengths of TLS in capturing realistic 3D forest structures and ensuring structure change traceability, offering critical insights for the quantification of forest structure and AGBC dynamics using multi-temporal TLS data.

CRediT authorship contribution statement

Shilin Chen: Writing – review & editing, Writing – original draft, Visualization, Validation, Project administration, Methodology, Formal analysis, Data curation, Conceptualization. **Hans Verbeeck:** Writing – review & editing, Supervision, Conceptualization. **Louise Terry:** Writing – review & editing, Supervision. **Wout Cherlet:** Writing – review & editing, Methodology. **Chang Liu:** Writing – review & editing, Investigation, Data curation. **Mathias Disney:** Writing – review & editing, Investigation, Funding acquisition, Data curation. **Yadvinder Malhi:** Writing – review & editing, Investigation, Data curation. **Niall Origo:** Writing – review & editing, Investigation, Data curation. **Joanne Nightingale:** Writing – review & editing, Investigation. **Kim Calders:** Writing – review & editing, Supervision, Methodology, Investigation, Conceptualization.

Declaration of competing interest

The authors declare that they have no known competing financial interests or personal relationships that could have appeared to influence the work reported in this paper.

Acknowledgements

The collection of the Wytham Woods TLS data was funded through the Metrology for Earth Observation and Climate project (MetEOC-2), grant number ENV55 within the European Metrology Research Program (EMRP) and capital funding from NERC National Centre for Earth Observation. The EMRP is jointly funded by the EMRP participating countries within EURRAMEP and the European Union. Shilin Chen is

financially supported by the China Scholarship Council [No.202209370016]. Wout Cherlet and Kim Calders are funded by the European Union (ERC-2021-STG Grant agreement No. 101039795). Views and opinions expressed are however those of the author(s) only and do not necessarily reflect those of the European Union or the

European Research Council Executive Agency. Neither the European Union nor the granting authority can be held responsible for them. MD acknowledges funding from the UK's NERC National Centre for Earth Observation (NCEO) and from NERC grant NE/T007648/1 "The multi-trophic impact of ash dieback".

Appendix A

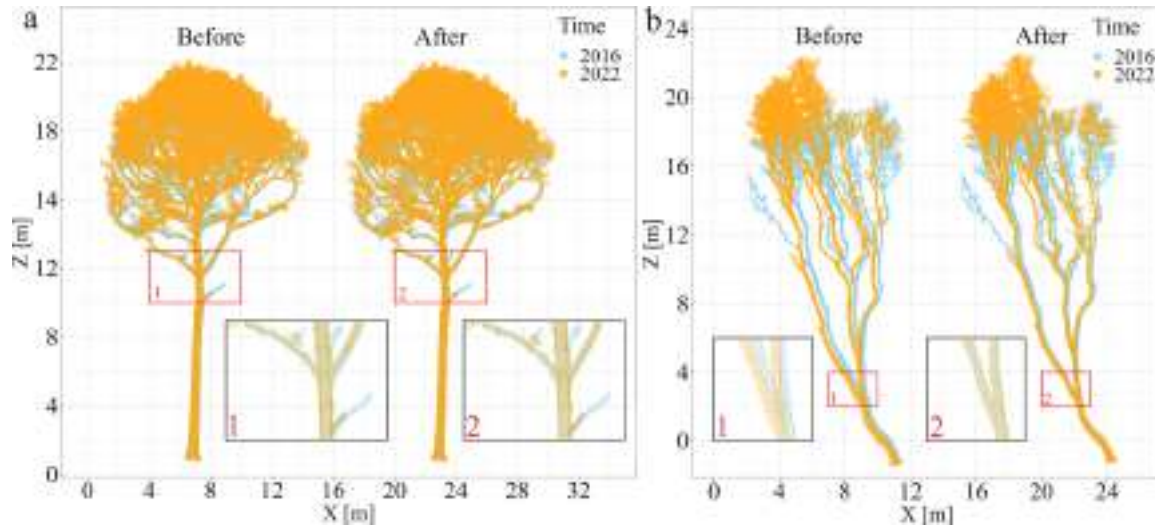


Fig. A1. Manual alignment of bi-temporal individual tree point clouds. 'Before' and 'After' represent the temporal point clouds before and after manual registration, respectively.

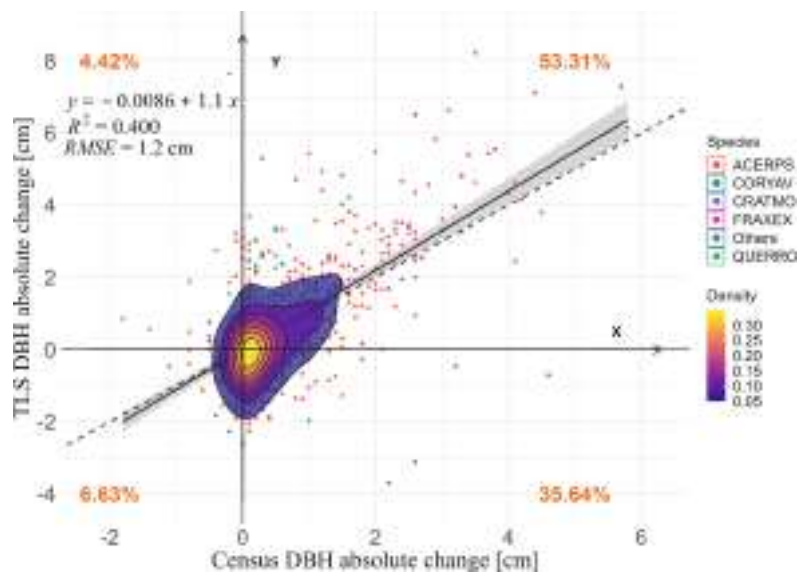


Fig. A2. Correlation between absolute changes in TLS-DBH and Census DBH. The orange numbers indicate the proportion of points within each quadrant relative to the total (679 trees).

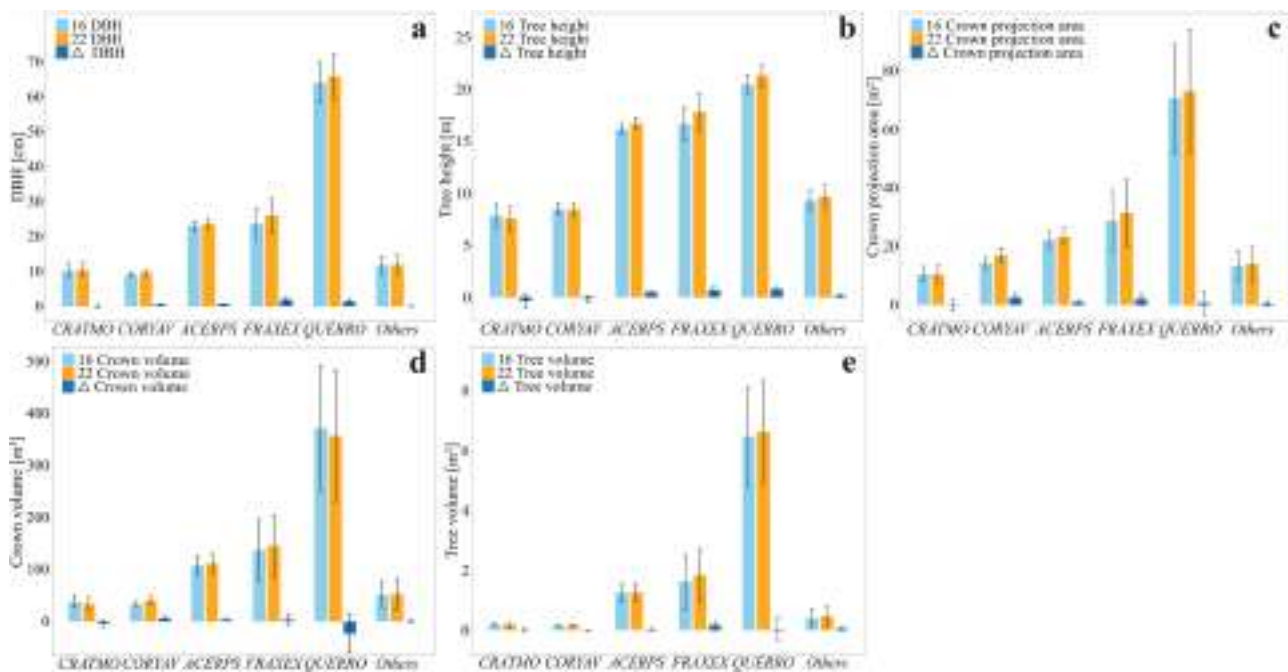


Fig. A3. Comparison of mean changes in per-tree forest structure metrics of different tree species at the plot-level from 2016 to 2022. a, b, c, d, e represent the mean changes over six years in the structural attributes: diameter at breast height (DBH), tree height, crown projection area, crown volume, and aboveground tree volume, respectively. The error bars indicate the standard error range of forest structural attributes within a 95 % confidence interval. ‘16’ and ‘22’ indicate the years 2016 and 2022, respectively. ‘ Δ ’ indicates the absolute change in forest structural attributes.

Data availability

Data will be made available on request.

References

- Astigarraga, J., et al., 2025. Forest structural diversity modulates tree growth synchrony in response to climate change. *Forest. Ecol. Manag.* 579.
- Bauwens, S., Bartholomeus, H., Calders, K., Lejeune, P., 2016. Forest inventory with terrestrial LiDAR: a comparison of static and hand-held mobile laser scanning. *Forests*. 7 (6).
- Bogdanovich, E., et al., 2021. Using terrestrial laser scanning for characterizing tree structural parameters and their changes under different management in a Mediterranean open woodland. *Forest. Ecol. Manag.* 486.
- Buras, A., Rammig, A., Zang, C.S., 2020. Quantifying impacts of the 2018 drought on European ecosystems in comparison to 2003. *Biogeosciences*. 17 (6), 1655–1672.
- Burt, A., Disney, M., Calders, K., 2019. Extracting individual trees from lidar point clouds using. *Methods Ecol. Evol.* 10 (3), 438–445.
- Butt, N., Campbell, G., Malhi, Y., Morecroft, M., Fenn, K., Thomas, M., 2009. Initial Results from Establishment of a Long-Term Broadleaf Monitoring Plot At Wytham Woods. University Oxford, Oxford, UK, Rep, Oxford, UK.
- Calders, K., et al., 2020. Terrestrial laser scanning in forest ecology: expanding the horizon. *Remote Sens. Environ.* 251.
- Calders, K., et al., 2025. Realistic virtual forests for understanding forest disturbances and recovery from space. *Isprs. J. Photogramm.* 227, 501–507.
- Calders, K., et al., 2015. Nondestructive estimates of above-ground biomass using terrestrial laser scanning. *Methods Ecol. Evol.* 6 (2), 198–208.
- Calders, K., et al., 2018. Realistic forest stand reconstruction from terrestrial LiDAR for radiative transfer modelling. *Remote Sens-Basel*. 10 (6).
- Calders, K., et al., 2022. Laser scanning reveals potential underestimation of biomass carbon in temperate forest. *Ecol. Solut. Evid.* 3 (4).
- Campos, M.B., et al., 2021. A long-term terrestrial laser scanning measurement station to continuously monitor structural and phenological dynamics of boreal forest canopy. *Front. Plant Sci.* 11.
- Chave, J., Coomes, D., Jansen, S., Lewis, S.L., Swenson, N.G., Zanne, A.E., 2009. Towards a worldwide wood economics spectrum. *Ecol. Lett.* 12 (4), 351–366.
- Chen, S., et al., 2025. The impact of leaf-wood separation algorithms on aboveground biomass estimation from terrestrial laser scanning. *Remote Sens. Environ.* 318, 114581.
- Coomes, D.A., Allen, R.B., 2007. Effects of size, competition and altitude on tree growth. *J. Ecol.* 95 (5), 1084–1097.
- Cooper, Z.T., et al., 2026. Benchmarking quantitative structure modelling algorithms against destructively sampled aboveground biomass estimates. *Remote Sens. Environ.* (under review).
- Coops, N.C., Irwin, L.A.K., Seely, H.S., Hardy, S.J., 2025. Advances in laser scanning to assess carbon in forests: from ground-based to space-based sensors. *Curr. for. Rep.* 11 (1).
- Dalponte, M., Jucker, T., Liu, S.C., Frizzera, L., Gianelle, D., 2019. Characterizing forest carbon dynamics using multi-temporal lidar data. *Remote Sens. Environ.* 224, 412–420.
- Demol, M., Calders, K., Verbeeck, H., Gielen, B., 2021. Forest above-ground volume assessments with terrestrial laser scanning: a ground-truth validation experiment in temperate, managed forests. *Ann. Bot-London* 128 (6), 805–819.
- Demol, M., et al., 2022. Estimating forest above-ground biomass with terrestrial laser scanning: current status and future directions. *Methods Ecol. Evol.* 13 (8), 1628–1639.
- Eitel, J.U.H., Vierling, L.A., Magney, T.S., 2013. A lightweight, low cost autonomously operating terrestrial laser scanner for quantifying and monitoring ecosystem structural dynamics. *Agr. Forest. Meteorol.* 180, 86–96.
- Fan, G.P., Nan, L.L., Dong, Y.Q., Su, X.H., Chen, F.X., 2020. AdQSM: a new method for estimating above-ground biomass from TLS point clouds. *Remote Sens-Basel* 12 (18).
- Feng, Y.H., et al., 2024. L1-Tree: a novel algorithm for constructing 3D tree models and estimating branch architectural traits using terrestrial laser scanning data. *Remote Sens. Environ.* 314.
- Fenn, K., Malhi, Y., Morecroft, M., Lloyd, C., Thomas, M., 2015. The carbon cycle of a maritime ancient temperate broadleaved woodland at seasonal and annual scales. *Ecosystems*. 18 (1), 1–15.
- Fu, X.Y., et al., 2021. Assessment of approaches for monitoring forest structure dynamics using bi-temporal digital aerial photogrammetry point clouds. *Remote Sens. Environ.* 255.
- Griebel, A., Bennett, L.T., Culvenor, D.S., Newnham, G.J., Arndt, S.K., 2015. Reliability and limitations of a novel terrestrial laser scanner for daily monitoring of forest canopy dynamics. *Remote Sens. Environ.* 166, 205–213.
- Hackenberg, J., Spiecker, H., Calders, K., Disney, M., Raunonen, P., 2015. SimpleTree-an efficient open source tool to build tree models from TLS clouds. *Forests* 6 (11), 4245–4294.
- Herranz, A.D., Salazar-Zarzosa, P.C., Mesas, F.J., Arenas-Castro, S., Ruiz-Benito, P., Villar, R., 2023. Modelling aboveground biomass and productivity and the impact of climate change in Mediterranean forests of South Spain. *Agr. Forest. Meteorol.* 337.
- Herrmann, S., Kahl, T., Bauhus, J., 2015. Decomposition dynamics of coarse woody debris of three important central European tree species. *For. Ecosyst.* 2.
- Husin, N.A., Khairunniza-Bejo, S., Abdullah, A.F., Kassim, M.S.M., Ahmad, D., 2022. Multi-temporal analysis of terrestrial laser scanning data to detect basal stem rot in oil palm trees. *Precis. Agric.* 23 (1), 101–126.
- Kirby, K.J., et al., 2014. Changes in the tree and shrub layer of Wytham Woods (Southern England) 1974–2012: local and national trends compared. *Forest: An Int. J. Forest Res.* 87 (5), 663–673.
- Knutzen, F., et al., 2025. Impacts on and damage to European forests from the 2018–2022 heat and drought events. *Nat. Hazards Earth Syst. Sci.* 25 (1), 77–117.

- Li, H.T., Hiroshima, T., Li, X.X., Hayashi, M., Kato, T., 2024. High-resolution mapping of forest structure and carbon stock using multi-source remote sensing data in Japan. *Remote Sens. Environ.* 312.
- Liang, X.L., Hyyppä, J., Kaartinen, H., Holopainen, M., Melkas, T., 2012. Detecting changes in forest structure over time with Bi-temporal terrestrial laser scanning data. *Isprs. Int. J. Geo-Inf.* 1 (3), 242–255.
- Liang, X.L., et al., 2018. International benchmarking of terrestrial laser scanning approaches for forest inventories. *Isprs. J. Photogramm.* 144, 137–179.
- Liang, X.L., et al., 2016. Terrestrial laser scanning in forest inventories. *Isprs. J. Photogramm.* 115, 63–77.
- Liu, C., et al., 2024. Bitemporal radiative transfer modeling using Bitemporal 3D-explicit forest reconstruction from terrestrial laser scanning. *Remote Sens.-Basel* 16 (19).
- Luoma, V., et al., 2021. Revealing changes in the stem form and volume allocation in diverse boreal forests using two-date terrestrial laser scanning. *Forests* 12 (7).
- Martin-Ducup, O., et al., 2020. Terrestrial laser scanning reveals convergence of tree architecture with increasingly dominant crown canopy position. *Funct. Ecol.* 34 (12), 2442–2452.
- Martin-Ducup, O., Schneider, S., Fournier, R.A., 2017. A method to quantify canopy changes using multi-temporal terrestrial lidar data: tree response to surrounding gaps. *Agr. Forest. Meteorol.* 237, 184–195.
- McCarley, T.R., et al., 2017. Multi-temporal LiDAR and Landsat quantification of fire-induced changes to forest structure. *Remote Sens. Environ.* 191, 419–432.
- McDowell, N.G., et al., 2020. Pervasive shifts in forest dynamics in a changing world. *Science* 368 (6494), 964. —+.
- Moeys, K., et al., 2025. Allometric equations underestimate woody volumes of large solitary trees outside forests. *Urban Forest. Urban Green.*, 128839
- Needham, J.F., et al., 2022. Tree crown damage and its effects on forest carbon cycling in a tropical forest. *Glob. Change Biol.* 28 (18), 5560–5574.
- Piponiot, C., et al., 2022. Distribution of biomass dynamics in relation to tree size in forests across the world. *New. Phytol.* 234 (5), 1664–1677.
- Pretzsch, H., 2010. Forest dynamics, growth and yield. *From Measure. Model* 1–664.
- Raunonen, P., et al., 2013. Fast automatic precision tree models from terrestrial laser scanner Data. *Remote Sens.-Basel.* 5 (2), 491–520.
- Schulte, M., Jonsson, R., Hammar, T., Stendahl, J., Hansson, P.A., 2022. Nordic forest management towards climate change mitigation: time dynamic temperature change impacts of wood product systems including substitution effects. *Eur. J. Forest. Res.* 141 (5), 845–863.
- Seidl, R., et al., 2017. Forest disturbances under climate change. *Nat. Clim. Change* 7 (6), 395–402.
- Shen, W.J., Li, M.S., Huang, C.Q., Tao, X., Wei, A.S., 2018. Annual forest aboveground biomass changes mapped using ICESat/GLAS measurements, historical inventory data, and time-series optical and radar imagery for Guangdong province, China. *Agr. Forest. Meteorol.* 259, 23–38.
- Srinivasan, S., Popescu, S.C., Eriksson, M., Sheridan, R.D., Ku, N.W., 2014. Multi-temporal terrestrial laser scanning for modeling tree biomass change. *Forest. Ecol. Manag.* 318, 304–317.
- Terryn, L., 2024. **Laser Scanning For Monitoring Tree Structure in Tropical Rainforests.** Ghent University. Faculty of Bioscience Engineering, Ghent, Belgium. <http://hdl.handle.net/1854/LU-01HM9QWX1NYKQM52NWX1GHX2HT>.
- Terryn, L., et al., 2023. Analysing individual 3D tree structure using the R package ITSM. *Methods Ecol. Evol.* 14 (1), 231–241.
- Terryn, L., et al., 2022. Quantifying tropical forest structure through terrestrial and UAV laser scanning fusion in Australian rainforests. *Remote Sens. Environ.* 271.
- Terryn, L., et al., 2020. Tree species classification using structural features derived from terrestrial laser scanning. *Isprs. J. Photogramm.* 168, 170–181.
- Thom, D., et al., 2022. Will forest dynamics continue to accelerate throughout the 21st century in the Northern Alps? *Glob. Change Biol.* 28 (10), 3260–3274.
- Vandendaele, B., Martin-Ducup, O., Fournier, R.A., Pelletier, G., 2024. Evaluation of mobile laser scanning acquisition scenarios for automated wood volume estimation in a temperate hardwood forest using quantitative structural models. *Can. J. Forest. Res.* 54 (7), 774–792.
- Wang, D., Puttonen, E., Casella, E., 2022. PlantMove: a tool for quantifying motion fields of plant movements from point cloud time series. *Int. J. Appl. Earth Obs.* 110.
- Wang, F., Jia, W., Li, F., 2025. Forest growth dynamics can be revealed using dual-temporal terrestrial laser Scanning — A case from plantation forests in northeastern China. *Urban Forest. Urban Green.* 114, 129155.
- Wilkes, P., et al., 2017. Data acquisition considerations for Terrestrial Laser scanning of forest plots. *Remote Sens. Environ.* 196, 140–153.
- Yrttimaa, T., et al., 2020. Structural changes in boreal forests can be quantified using terrestrial laser scanning. *Remote Sens.-Basel.* 12 (17).
- Yrttimaa, T., et al., 2022. Exploring tree growth allometry using two-date terrestrial laser scanning. *Forest. Ecol. Manag.* 518.
- Zhao, K.G., Suarez, J.C., Garcia, M., Hu, T.X., Wang, C., Londo, A., 2018. Utility of multitemporal lidar for forest and carbon monitoring: tree growth, biomass dynamics, and carbon flux. *Remote Sens. Environ.* 204, 883–897.
- Zuleta, D., et al., 2023. Damage to living trees contributes to almost half of the biomass losses in tropical forests. *Glob. Change Biol.* 29 (12), 3409–3420.